APL/JHU
TG 1293A
JULY 1976
Copy No. 1

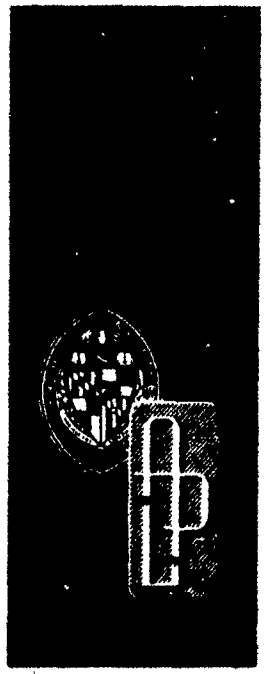

Technical Memorandum

URLIM—A UNIFIED RADOME LIMITATIONS COMPUTER PROGRAM, VOLUME 1—THEORETICAL BACKGROUND

R. K. FRAZER

THE JOHNS HOPKINS UNIVERSITY ■ APPLIED PHYSICS LABORATORY

APL/JHU
TG 1293A
JULY 1976

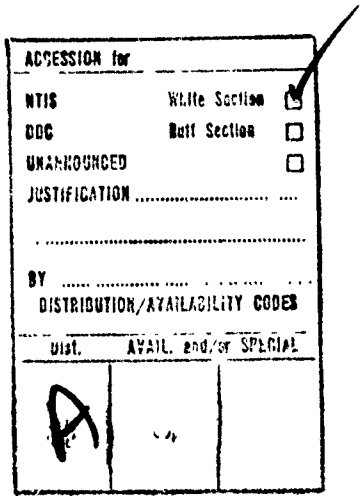

Technical Memorandum

URLIM—A UNIFIED RADOME LIMITATIONS COMPUTER PROGRAM, VOLUME 1—THEORETICAL BACKGROUND

R. K. FRAZER

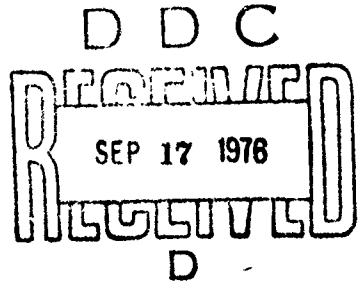

THE JOHNS HOPKINS UNIVERSITY ■ APPLIED PHYSICS LABORATORY
Johns Hopkins Road, Laurel, Maryland 20810

PLEASE FOLD BACK IF NOT NEEDED FOR BIBLIOGRAPHIC PURPOSES

REPORT DOCUMENTATION PAGE

1. REPORT NUMBER: APL/JHU/TG-1293A-Vol-1	2. GOVT ACCESSION NO
3. RECIPIENT'S CATALOG NUMBER	
4. TITLE (and Subtitle): URLIM - A UNIFIED RADOME LIMITATIONS COMPUTER PROGRAM, VOLUME 1, THEORETICAL BACKGROUND	5. TYPE OF REPORT & PERIOD COVERED: Technical Memo
	6. PERFORMING ORG. REPORT NUMBER
7. AUTHOR(s): R. K. Frazer	8. CONTRACT OR GRANT NUMBER(s): N00017-72-C-4401
9. PERFORMING ORGANIZATION NAME & ADDRESS: The Johns Hopkins University Applied Physics Laboratory, Johns Hopkins Rd., Laurel, MD 20810	10. PROGRAM ELEMENT, PROJECT, TASK AREA & WORK UNIT NUMBERS: Task A33
11. CONTROLLING OFFICE NAME & ADDRESS: Naval Plant Representative Office, Johns Hopkins Rd., Laurel, MD 20810	12. REPORT DATE: July 1956 13. NUMBER OF PAGES: 93
14. MONITORING AGENCY NAME & ADDRESS: Naval Plant Representative Office, Johns Hopkins Rd., Laurel, MD 20810	15. SECURITY CLASS. (of this report): Unclassified 15a. DECLASSIFICATION/DOWNGRADING SCHEDULE

16. DISTRIBUTION STATEMENT (of this Report)

Approved for public release; distribution unlimited.

17. DISTRIBUTION STATEMENT (of the abstract entered in Block 20, if different from Report)

18. SUPPLEMENTARY NOTES

19. KEY WORDS (Continue on reverse side if necessary and identify by block number)

aerodynamic heating
boresight errors
heat transfer
missiles
radomes
thermal stresses
trajectory simulation

20. ABSTRACT (Continue on reverse side if necessary and identify by block number)

URLIM, a unified radome limitations computer program, has been developed to aid the radome design engineer by providing a definition of the maximum flight performance capabilities of radome materials. URLIM numerically determines the response of the radome to aerodynamic heating and loading. It computes the following as functions of trajectory time: thermal stress; radar boresight error rates; missile-radome attachment stresses caused by maneuvers, pressure, and drag forces; and the onset of radome melting. The basic output of the program is a notation of trajectory time at which the radome reaches its design limitations. Many options are available to the user of the URLIM program that provide a wide variety of analysis capability. For this reason, URLIM may also be considered as a general purpose aerodynamic heat transfer program as well as a specific purpose radome limitations program. Volume 1 of this report presents the theoretical background of the analysis techniques used in URLIM; Volume 2 provides a detailed explanation of how to use URLIM.

DD FORM 1 JAN 73 1473

031650

THE JOHNS HOPKINS UNIVERSITY
APPLIED PHYSICS LABORATORY
LAUREL, MARYLAND

ABSTRACT

URLIM, a unified radome limitations computer program, has been developed to aid the radome design engineer by providing a definition of the maximum flight performance capabilities of radome materials. URLIM numerically determines the response of the radome to aerodynamic heating and loading. It computes the following as functions of trajectory time: thermal stress; radar boresight error rates; missile-radome attachment stresses caused by maneuvers, pressure, and drag forces; and the onset of radome melting. The basic output of the program is a notation of trajectory time at which the radome reaches its design limitations. Many options are available to the user of the URLIM program that provide a wide variety of analysis capability. For this reason, URLIM may also be considered as a general purpose aerodynamic heat transfer program as well as a specific purpose radome limitations program. Volume 1 of this report presents the theoretical background of the analysis techniques used in URLIM; Volume 2 provides a detailed explanation of how to use URLIM.

PREFACE

The purpose of this volume is to present the theoretical background of the analysis techniques used in the URLIM program. This discussion will consist of three basic parts: first, it will present the mathematical relationships between variables, along with their assumptions and limitations; second, it will describe the numerical techniques employed by the program to solve the various equations; third, it will outline the data management techniques used to find the various solutions. The first section describes the physical models that are the analytical basis of the program. As such, this section provides a view of URLIM that will enable the prospective user to assess the accuracy and completeness of the facilities provided in the program. The last two sections will provide an overview of the URLIM program organization that may give the interested user an insight to the generality of the code. Moreover, as errors will inevitably occur, this level of understanding of the program's organization will serve as an aid to debugging.

CONTENTS

ILLUSTRATIONS

1. THEORETICAL BASIS

HEAT TRANSFER -- CONDUCTION

The unified radome limitations computer program (URLIM) was developed to predict heat transfer within a solid. Fundamentally, the determination of the time-dependent temperature field within a closed volume will depend on the rate of heat conducted orthogonally across the surface of the volume and the rate of change of internal energy within the volume. We will assume the arbitrary case of a volume V with some temperature existing at every point within V. In the absence of any effects from electric or magnetic fields, surface tension, or chemical reactions, the energy in a solid is a function of its temperature such that

$$\frac{du}{dt} = \frac{\partial(\rho c_p T)}{\partial t} \quad , \tag{1}$$

where

du/dt is the time rate of change of internal energy in a differential volume, dV,

ρ is the density of the material,

c_p is the specific heat of the material,

T is the magnitude of the temperature field at the differential volume dV (i.e., the temperature of dV), and

t is the independent variable time.

The movement of heat through any point in the volume is related to the gradient of the temperature field within the volume; that is,

$$\bar{Q} = -k\bar{\nabla}T \quad , \tag{2}$$

where

$\bar{Q}$ is the heat flow vector,

$\bar{\nabla}T$ is the temperature field gradient vector, and

k is the proportionality factor that can only be a function of temperature (i.e., $k = f(T)$).

Equation (2) states that heat flows within a solid in the opposite direction to the temperature gradient and that the magnitude of that flow is related by the material property k, which may be temperature dependent.

With Equation (2) describing the flow of heat at any point in the volume, the divergence of the vector $\bar{Q}$ is written as

$$\bar{\nabla} \cdot \bar{Q} = \bar{\nabla} \cdot k\bar{\nabla}T \quad , \tag{3}$$

and is thought of as the change in magnitude of heat flow with respect to any point in the volume. In a conservative system (as has been assumed here) this spatial change in heat flow at a point in the volume is equal to the temporal change in internal energy of that point. Using Eqs. (1) and (3) the following equation represents this statement of the conservation of energy:

$$\bar{\nabla} \cdot k\bar{\nabla}T = -\frac{\partial(\rho c_p T)}{\partial t} \tag{4a}$$

The material property product (ρc_p) is allowed to depend explicitly only on temperature (i.e., $\rho c_p = f(T)$), so that

$$\bar{\nabla} \cdot k\bar{\nabla}T = -\rho c_p \frac{\partial T}{\partial t} \quad . \tag{4b}$$

The operator $\bar{\nabla}$ is the vector gradient operator and must be represented in an orthogonal coordinate system. It can have the following definitions.

Cartesian Coordinates:

$$\bar{\nabla} = \frac{\partial}{\partial x}\hat{i} + \frac{\partial}{\partial y}\hat{j} + \frac{\partial}{\partial z}\hat{k} \quad , \tag{5}$$

where $\hat{x}$, $\hat{y}$, and $\hat{z}$ are the unit vectors in each of the coordinate directions.

Cylindrical Coordinates:

$$\nabla = \frac{\partial}{\partial r}\hat{r} + \frac{1}{r}\frac{\partial}{\partial \theta}\hat{\theta} + \frac{\partial}{\partial z}\hat{z} \quad , \tag{6}$$

where

r is the radial coordinate,

θ is the circumferential coordinate, and

z is the axial coordinate.

Spherical Coordinates:

$$\nabla = \frac{\partial}{\partial r}\hat{r} + \frac{1}{r}\frac{\partial}{\partial \phi}\phi + \frac{1}{r \sin \phi}\frac{\partial}{\partial \theta}\hat{\theta} \quad , \tag{7}$$

where

r is the radial coordinate,

ϕ is the co-latitudinal coordinate, and

θ is the longitudinal coordinate.

Equation (4) is the governing relationship between the spatial and temporal changes of temperature within the body. Specific solutions to the sets of differential equations indicated in Eq. (4) depend on the specification of the conditions that exist at the boundary surface of the volume and whether or not there are independent heat sources or sinks present within the volume. Section 2 of this volume will show how the general relationships expressed here are modeled and the temperature field solved for as a function of time.

HEAT TRANSFER -- CONVECTION

In situations where the volume being considered is subjected to a fluid flowing at its surface, heat transfer will occur across

the surface due to conduction within the fluid, viscous friction dissipation within the fluid near the surface, and molecular motion in the boundary layer (i.e., convection). In general, the static temperature of the fluid and the surface temperature of the solid will be different and there will be a potential for moving heat across the surface. Figure 1 shows a schematic diagram of a fluid flowing past a solid surface with an appropriate coordinate system and with the important parameters listed. If the bulk of the fluid stream in the vicinity of the surface is hotter than the surface, there will be a spatial variance of temperature through the stream as shown in the figure. Due to the viscous effects of the fluid, the fluid particles at the wall surface will be assumed stationary with respect to the wall. The velocity and temperature variances as one travels away from the wall are as shown in the figure. The points at which the velocity and temperature of the gas reach 99% of their freestream values describe the boundary layer edge; the two points (one for temperature and one for velocity) will be assumed to coincide spatially at every point along the body. The maximum boundary layer temperature is called the "recovery" or "adiabatic wall" temperature and is defined as the fluid temperature where the derivative with respect to the local wall normal ($\partial T_f/\partial y$) is zero.

Predictions of the aerodynamic heating as described so far involve calculating the recovery temperature and estimating the proper dependence of the convective flux ($\dot{q}$) on the recovery temperature. In the discussions that follow, the basic relation shown below will be used to define the heat flux per unit area to the solid surface:

$$\dot{q}_w = h_i(i_r - i_w) \ , \tag{8}$$

where

h_i is a heat transfer coefficient that will relate heat flow to a difference in enthalpy,

i_r is the enthalpy of the fluid at the recovery temperature, and

i_w is the enthalpy of the fluid at the wall temperature.

Enthalpy, a valid material property, is defined as

$$i = u + pv,$$

where u is the internal energy, p the pressure, and v the specific volume (reciprocal of density). Enthalpy is, in general,

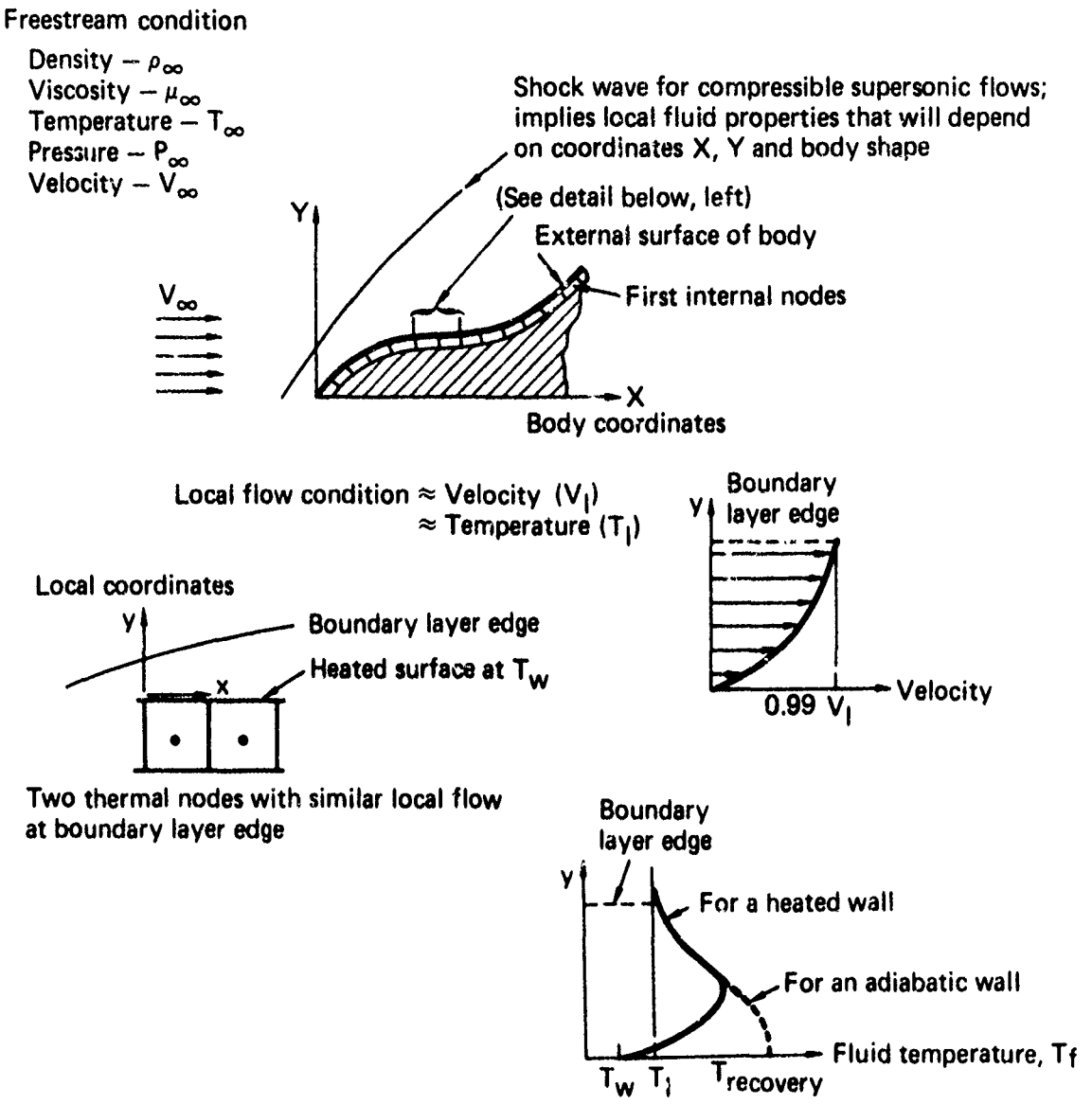

Fig. 1 Terminology for Aerodynamic Heating Boundary Conditions

dependent on temperature and pressure. We will assume knowledge of the fluid properties, including enthalpy versus fluid temperature (T_f) and fluid pressure (P_f), so that it remains to calculate h_i and the recovery enthalpy. In the following discussion the fluid will be assumed to be a gas (usually air).

With a compressible fluid as the medium there is the possibility that the freestream velocity is larger than the acoustic velocity in the gas and a shock wave may be present in the vicinity of the wall surface being considered. If this is the case, the local boundary layer edge velocity (V_1) must first be calculated. This calculation involves a priori knowledge of the ratio of pressures across the shock wave as well as the ratio of Mach numbers. (The Mach number (M) is the ratio of actual gas velocity to the acoustic velocity of the gas at any point.) Further, the distance from the shock wave to the local body position and the shape of the body have effects on the Mach and pressure ratios mentioned here. In other words,

$$P_1/P_0 = f(M_0,x) \quad \text{and} \tag{9}$$

$$M_1/M_0 = g(M_0,x) \ , \tag{10}$$

with x indicating the position along the body, 1 indicating the local condition, 0 indicating the freestream condition, and the other items as shown in Fig. 1. Since energy is conserved across a shock wave, the following equation will hold:

$$i_1 + \frac{V_1^2}{2} = i_0 + \frac{V_0^2}{2} \ , \tag{11}$$

which simply sums the sensible and kinetic energies on either side of the shock wave. If the gas is assumed to be ideal except for a compressibility factor (Z) defined as

$$Z = pv/RT,$$

then the sonic velocity (a) can be shown to be

$$a = \sqrt{\gamma g Z R T} \ , \tag{12}$$

where

γ is the ratio of specific heats (c_p/c_v) for the gas, which are defined as

$$c_p = di/dT \text{ and}$$

$$c_v = du/dT \ .$$

The gas properties γ and Z will be assumed to be known as functions of temperature and pressure. Using the above definitions Eq. (11) is written as

$$i_1 + \frac{\gamma_1 Z_1 R T_1 M_1^2}{2} = i_0 + \frac{V_1^2}{2} \ . \tag{13}$$

With knowledge of the freestream conditions of temperature and pressure, the gas properties i, γ, Z, and the functions indicated by Eqs. (9) and (10), Eq. (13) is seen as an implicit equation in T_1.

When Eq. (13) is solved for T_1, the local flow conditions are then fully defined and the recovery condition is next considered. The recovery temperature within the boundary layer must lie somewhere between the total temperature and the local boundary layer edge temperature. Thinking in terms of enthalpy instead of temperature this notion is expressed as

$$i_r = i_1 + r \frac{V_1^2}{2} \ , \tag{14}$$

where r is the recovery factor, defined as

$$r = \frac{T_r - T_0}{T_\infty - T_0} \ . \tag{15a}$$

To determine r it is necessary to resort to empirical correlations of measured data. Reference 1 states the following relationship for r:

$$r = \sqrt{Pr^*} \text{ for laminar flow} \tag{15b}$$

Ref. 1. R. E. Wilson, Handbook of Supersonic Aerodynamics, Sections 13 and 14, "Viscosity" and "Heat Transfer Effects," NAVORD Report 1488, Naval Ordnance Laboratory, White Oak, MD, August 1966.

$$r = \sqrt[3]{Pr^*} \text{ for turbulent flow,} \tag{15c}$$

where Pr* is the Prandtl number of the airstream evaluated at the reference temperature (reference denoted by *) and the Pr number is

$$Pr = c_p \mu/k ,$$

μ being the viscosity. We have now traded one unknown for another; that is, the recovery factor is defined in terms of another unknown condition — the reference temperature (T*). The reference temperature is a fictitious boundary layer temperature that is used to evaluate the physical properties of the stream. Eckert (Ref. 2) proposes the following relationship for determining the reference condition in terms of enthalpies:

$$i^* = (i_w + i_1 + 0.22\ r\ V_1^2)/2 , \tag{16}$$

which is seen to be an average of enthalpies and a kinetic energy factor. Equation (16) now involves the recovery factor so an explicit solution for r from Eqs. (14), (15), and (16) cannot be made; the relationships must be solved simultaneously.

The results of solving Eqs. (14) through (16) are the reference enthalpy (i^*) and the recovery enthalpy (i_r). By use of the fluid property tables the reference and recovery enthalpies can be used to obtain the reference and recovery temperatures (T* and T_r, respectively). At this point we can turn to heat transfer correlations to evaluate the h_i of Eq. (8). The Stanton number is defined as

$$St = \frac{\dot{q}}{\rho^* V_1 (i_r - i_w)} = \frac{h_i}{\rho^* V_1} , \tag{17}$$

Ref. 2. E. R. G. Eckert, "Survey of Boundary Layer Heat Transfer at High Velocities and High Temperatures," Technical Report 59-624, Wright Air Development Center, Dayton, OH, April 1960.

and Colburn (Ref. 3) notes that

$$St = c_f \, (Pr^*)^{\beta'} \quad . \tag{18}$$

The term c_f is the friction factor and is further defined as

$$c_f = \frac{\tau_w}{\rho V_1^{\,2}/2g_c} \quad , \tag{19}$$

where

τ_w is the stream shear stress at the wall surface,

g_c is 32.174 ft-lbm/lbf-s^2, and

β' is an empirical constant.

Experimental correlations (Refs. 2 and 3) have shown that

$$c_f = C \, Re^{\alpha'} \quad , \tag{20}$$

where C and α' are again empirical constants, and Re is the Reynolds number ($\rho V_1 x/\mu$). Combining Eqs. (17), (18), and (20) gives

$$\frac{h_i}{\rho^* V_L} = C \, Re^{\alpha'} \, Pr^{*\beta'} \quad . \tag{21a}$$

Using the definitions for Re and Pr, and the following for Nusselt number:

$$Nu = (c_p \times h_i)/k \quad ,$$

Ref. 3. A. P. Colburn, "A Method of Correlating Forced Convection Heat Transfer Data and a Comparison with Fluid Friction," Trans. AIChE, Vol. 29, 1933, pp. 174-210.

the general relationship

$$Nu = C\ Re^{\alpha}\ Pr^{\beta} \tag{21b}$$

can be written where the constants α and β are different from α' and β' and are given values according to Table 1.

Given the position on the body (x); the previously calculated values for T_r, T^*, and V_1; and the stream property functions; Eq. (21) or (21a) is solved for h_i and Eq. (8) is used to find the heat flux to the wall ($\dot{q}_w$).

In summary, the following steps are required to calculate $\dot{q}_w$:

1. Know i, Z, γ, Pr, and μ for the stream fluid versus T and P;

2. Know the Mach and pressure ratios (Eqs. (9) and (10)) between the freestream and the local boundary layer edge;

3. Calculate the local boundary layer edge static temperature (T_1) from Eq. (13);

4. Solve for the recovery factor (r), recovery temperature (T_r), and reference condition (T^*) (Eqs. (14), (15), (16));

5. Using properties at the reference temperature, solve for h_i using Eq. (21); and

6. Substitute h_i, i_r, and i_w in Eq. (8) to solve for $\dot{q}_w$.

Whether the laminar or turbulent coefficients in Table 1 are used depends generally on the value of the Reynolds number; low Re implies laminar flow and high Re implies turbulent. The transition value of Re must be decided a priori.

In the case of heating of a surface that is normal to the freestream (i.e., stagnation points) the methods of Squire and Sibulkin are used (Refs. 6 and 7). In these techniques it is

Ref. 6. S. Goldstein, Modern Developments in Fluid Dynamics, First Edition, Vol. 2, Oxford Univ. Press, London, 1938, p. 631.

Ref. 7. M. Sibulkin, "Heat Transfer near the Forward Stagnation Point of a Blunt Body," J. Aeronautical Sciences, August 1952.

Table 1

Constants for Nusselt Equation (Eq. (21b))

Type of Flow Field	α		C^*		β	r	
	Laminar	Turbulent	Laminar	Turbulent	Laminar and Turbulent	Laminar	Turbulent
Flat plate, Refs. 2 and 3	0.5	0.8	0.332	0.0296	0.333	$\sqrt{Pr^*}$	$\sqrt[3]{Pr^*}$
Cone, Ref. 1	0.5	0.8	0.575	0.0348	0.333	$\sqrt{Pr^*}$	$\sqrt[3]{Pr^*}$
Pipe flow, Refs. 4 and 5	0.4	0.8	$1.36\ (d/L)^{0.4}$	0.023	0.4	$\sqrt{Pr^*}$	$\sqrt[3]{Pr^*}$
2-d stagnation flow, Ref. 6	0.5	0.5	$0.570\sqrt{V_{grad}}$	$0.570\sqrt{V_{grad}}$	0.4	1	1
3-d stagnation flow, Ref. 7	0.5	0.5	$0.763\sqrt{V_{grad}}$	$0.763\sqrt{V_{grad}}$	0.4	1	1

* d/L is the entrance length ratio; d is the pipe diameter and L is the distance from the entrance defined in the accompanying text

Ref. 4. W. H. McAdams, Heat Transmission, McGraw-Hill, 1954.

Ref. 5. F. W. Dittus and L. M. K. Boelter, Publications in Engineering (University of California, Berkeley Campus), Vol. 2, 1930, p. 433.

possible to show that if the square root of the stream velocity gradient at the stagnation point is incorporated in the constant C (Table 1) then proper correlation with measured data is obtained. In these stagnation point heating cases, it was found that the term

$$V_{grad} = V'D/V_\infty$$

was required in the constant C of Eq. (21) where

- V' is $(\partial V/\partial y)|y = 0$, or the velocity gradient of the stream evaluated at the wall (c.f. Fig. 1),
- D is the characteristic diameter of the body, and
- V_∞ is the freestream velocity.

The dependence of V' on Mach number has been derived for a real gas using Newtonian flow assumptions. This plot is given in Fig. 2 and will be required for use when stagnation point heating is being considered.

The aerodynamic heat transfer relationships discussed above are solved in the SAERO routine where the final result is simply the temperature for the surface node in question. The temperature is solved for by making an energy balance at the heated surface per unit area as follows (c.f. Fig. 1):

$$\dot{q}_w + \dot{q}_{rad} = \sigma\varepsilon_w T_w^4 + \dot{q}_{con} ,$$

where:

- $\dot{q}_{rad}$ is an independently specified heat flux to the surface,
- T_w is the wall temperature,
- $\dot{q}_{con}$ is the heat conducted from the surface into the material below the surface,
- σ is the Stephan-Boltzmann constant (see the following section on radiation heat transfer), and
- ε_w is the total normal emissivity of the wall surface.

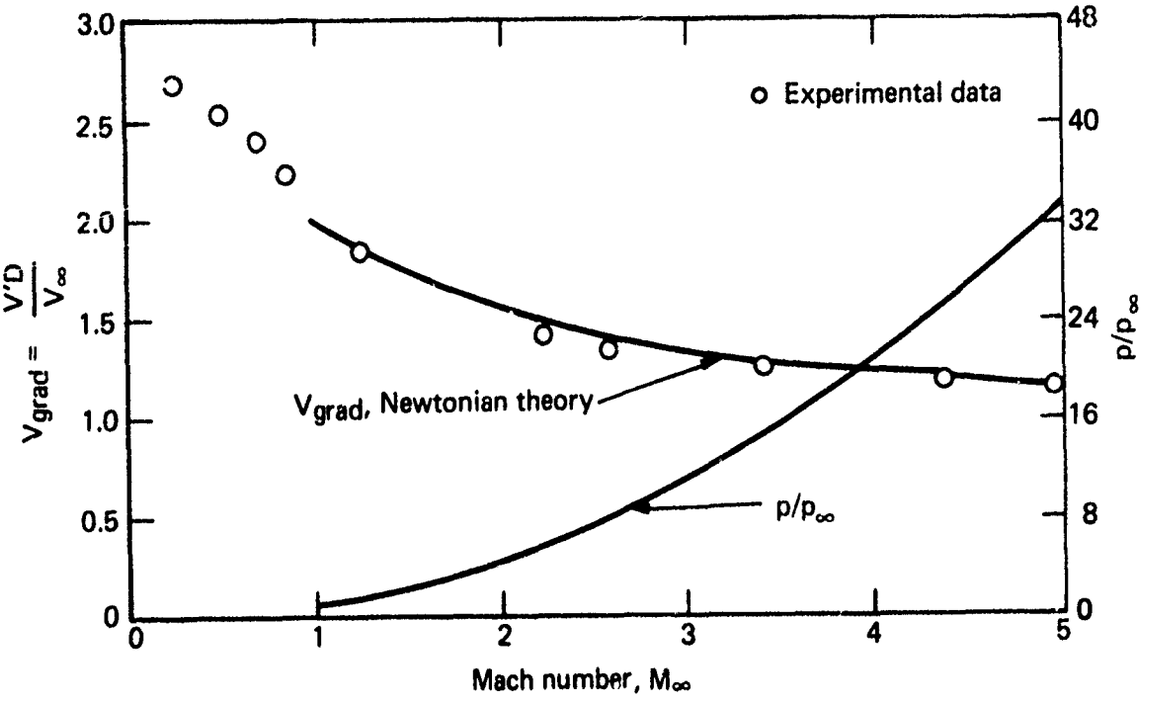

Fig. 2a Stagnation Point Velocity Gradient Function Comparison of Newtonian Theory with Experimental Data

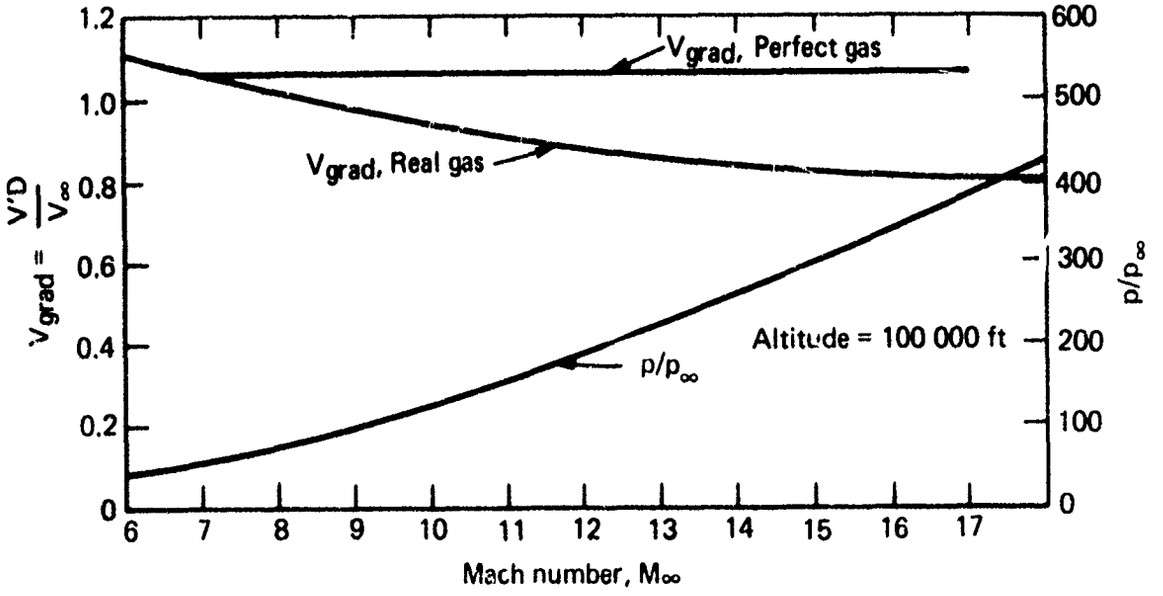

Fig. 2b Real Gas Effect on Stagnation Point Velocity Gradient Function

In this relationship, $\dot{q}_w$ (the aerodynamic heat transfer to the wall) is explicitly related to T_w through the enthalpy i_w (c.f. Eq. (8)). $\dot{q}_{rad}$ is independently specified and is therefore a constant at any instant in time. T_w^4 is an obvious function of T_w, and $\dot{q}_{con}$ depends on T_w as follows:

$$\dot{q}_{con} = k_w (T_w - T_i)/L_{w-i} \quad ,$$

where T_i is the inner wall temperature within a node at a distance L_{w-i} from the surface. The energy balance equation above is then seen as an implicit equation in T_w, if it is assumed that T_i is known. At each time increment in the transient solution technique the temperature T_i from the previous time point is used so that the conduction equation just above can be solved for $\dot{q}_{con}$ and the energy balance equation can be solved for T_w.

At this point we will also note that the solution for r, T_r, and T^* (Eqs. (14), (15a), and (16)) is made an explicit relation in the same way as the internal conduction equation. That is, the term r (Eq. (15a)) is used from a previous time step so that i_r (Eq. (14)) and i^* (Eq. (16)) are found without the need for a simultaneous solution of the three equations.

HEAT TRANSFER — RADIATION

Every substance at any temperature above absolute zero emits electromagnetic (EM) wave energy that will cause heat to be absorbed by any other surface upon which the energy impinges. Heat is, on an atomic level, a measure of the intensity of molecular vibrations. The molecules in a solid are groups of positive and negative electrical charges so their vibration at a surface will cause EM radiation. Conversely, EM waves of the proper frequency impinging on a surface will excite the molecular vibrations of that surface. In 1879 Stephan observed the following relationship for the energy flux radiated by a body at temperature T with a perfect surface (that is, a surface that emits the EM radiation without loss):

$$E_b = \sigma T^4 \quad . \qquad (22a)$$

Equation (22a) was also theoretically derived by Boltzmann and is termed the Stephan-Boltzmann law; σ is the Stephan-Boltzmann

constant. For real surfaces, the amount of energy radiated is less than the amount given by Eq. (22a) and an emissivity factor (ε) is generally incorporated:

$$E_g = \varepsilon\sigma T^4 \quad . \tag{22b}$$

The subscripts b and g in Eqs. (22a) and (22b), respectively, represent "black-body" (perfect) and "grey-body" (imperfect) surfaces, respectively. Because solid bodies are aggregates of molecules that are subject to the laws of quantum physics and quantum probabilities, the energy emitted at a particular temperature will be distributed over a wide range of wavelengths; i.e., the surface molecules vibrate over a range of frequencies. In 1900 Plank derived the following relation for the energy emitted at a specific wavelength by a body at a temperature T (c.f. Chapter 5 of Ref. 8)

$$E_{b\lambda} = \frac{C_1\lambda^{-5}}{\exp(C_2/\lambda T) - 1} \quad , \tag{23}$$

where C_1 and C_2 are constants. Equation (22a) is then seen as an integration of Eq. (23) over all wavelengths; i.e.,

$$E_b = \sigma T^4 = \int_0^\infty E_{b\lambda}\, d\lambda = C_1 \int_0^\infty \frac{\lambda^{-5}}{\exp(C_2/\lambda T) - 1}\, d\lambda \quad .$$

The implication of Eq. (23) is that for real surfaces the emissivity may, in general, exhibit a dependence on λ and T since a surface could be more emissive at one wavelength than another.

For a surface exposed to the EM radiation from another hot body the fraction absorbed (α) is related to the fraction reflected (r) and transmitted (τ) by a simple expression of the conservation of energy:

Ref. 8. F. Kreith, Principles of Heat Transfer, Second Edition, Section 5, International Textbook Co., Scranton, PA, 1965.

$$\alpha + \tau + r = 1$$

where

α is the absorptivity,

τ is the transmissivity, and

r is the reflectivity,

all of which may depend on T and λ.

In practical situations where radiation heat transfer is significant, the range of temperatures are such that the wavelengths of the EM energy involved are roughly between 0.5×10^{-6} and 20×10^{-6} m. This EM waveband is termed the infrared (IR) band. A simplifying assumption that will be made here is that all real materials ha values of r, ε, and α that are constant over the IR band and can depend only on the temperature of the surface. Further, the so called grey-body assumption will be made; that is, at a given temperature the emissivity of a material will be equal to the absorptivity. Given these assumptions, the net exchange of heat energy between the two surfaces shown below can be described.

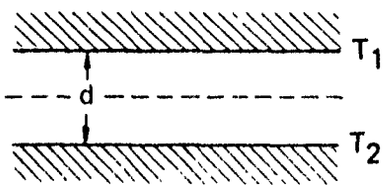

Let $T_1 > T_2$

It is desired to know the net heat flux per unit area ($\dot{q}_{net}$) across the imaginary plane spaced between the two given planes. This flux will be the total radiated heat per unit area from the surface at T_1 less the heat radiated from the surface at T_2 plus a consideration for the energy reflected at each surface. In algebraic terms:

$$\dot{q}_{net} = \varepsilon\sigma T_1^4 - \varepsilon\sigma T_2^4 + (1-\alpha)\varepsilon\sigma T_2^4 -$$

$$(1-\alpha)\varepsilon\sigma T_1^4 + (1-\alpha)^2 \varepsilon\sigma T_1^4 - (1-\alpha)^2\varepsilon\sigma T_2^4 + \ldots \quad (24)$$

The first two terms are the primary radiation terms, the third term represents the heat radiated by surface 2 but reflected at surface 1, the fourth term is the heat similarly reflected from surface 2, and the successive terms represent the continuing reflections that proceed indefinitely. Equation (24) can be simplified to:

$$\dot{q}_{net} = \varepsilon\sigma\left[T_1^4 - T_2^4 + T_1^4 \sum_{n=1}^{\infty} (1-\alpha)^n (-1)^n - T_2^4 \sum_{n=1}^{\infty} (1-\alpha)^n (-1)^n\right] , \quad (25a)$$

or

$$\dot{q}_{net} = \varepsilon\sigma \left(T_1^4 - T_2^4\right) \sum_{n=0}^{\infty} (1-\alpha)^n (-1)^n . \quad (25b)$$

The infinite sum is equal to:

$$\sum_{n=0}^{\infty} (1-\alpha)^n (-1)^n = \frac{1}{2-\alpha} . \quad (26)$$

Using the assumption that $\alpha = \varepsilon$, and

$$T_1^4 - T_2^4 \approx 4\,\bar{T}^3 (T_1 - T_2) ,$$

then Eq. (25a) becomes

$$\dot{q}_{net} = \frac{\varepsilon\sigma\bar{T}^3}{(2 - \varepsilon)} (T_1 - T_2) , \tag{27a}$$

where $\bar{T}^3 = (T_1 + T_2)\left(T_1^2 + T_2^2\right)$.

If we now consider the distance between the surfaces (d) and rewrite Eq. (27a) as

$$\dot{q}_{net} = \left[\frac{\varepsilon\sigma\bar{T}^3 d}{(2 - \varepsilon)}\right] \frac{(T_1 - T_2)}{d} , \tag{27b}$$

then the term in the square brackets can be regarded as the "effective" thermal conductivity of the space (d) between 1 and 2; i.e.,

$$\dot{q}_{net} = k_{eff} \frac{\Delta T}{d} ,$$

with

$$k_{eff} = \frac{\varepsilon\sigma\bar{T}^3 d}{(2 - \varepsilon)} . \tag{27c}$$

The above treatment is for parallel, infinite plates but similar analyses can be done considering the geometrical differences for arbitrary surfaces and the result is to add another factor called the view factor (F) to Eq. (27b); i.e.,

$$k_{eff} = \frac{\varepsilon\sigma\bar{T}^3 F}{(2 - \varepsilon)} . \tag{27d}$$

Values of F have been tabulated for various conventional surface arrangements; Ref. 8 gives some typical values.

While Eq. (27d) gives an effective conductivity for a linearized temperature function, Eq. (25b) could just as well be written

$$\dot{q}_{net} = \varepsilon_{eff}\, \sigma\left(T_1^4 - T_2^4\right) ,$$

with

$$\varepsilon_{eff} = \varepsilon/(2 - \varepsilon).$$

In Section 2 of this volume the solutions to these relationships will depend on having the values ε_{eff} mentioned above supplied a priori.

THERMAL STRESSES

Subroutines in URLIM can calculate thermal stresses in arbitrarily defined cylindrical wall sections. The method employed is that of Rivello (Ref. 9) and is briefly described here.

A cylinder of infinite length subdivided into n concentric cylindrical sections is shown schematically in Fig. 3. Also shown in Fig. 3 is a definition of the terms used in this discussion. The following assumptions are made:

1. The elastic modulus relating the stress in the material to the strain is constant within each region.
2. Poisson's ratio is constant throughout all regions.
3. The materials that may make up the cylinder are isotropic.
4. The cylinder is restrained from motion in the axial direction; i.e., the axial strain is zero at all values of r.
5. The radial distribution of temperature is known at all values of radius.

Ref. 9. R. M. Rivello, "Thermal Stress Analysis of Sandwich Cylinders," APL/JHU TG 721, August 1965.

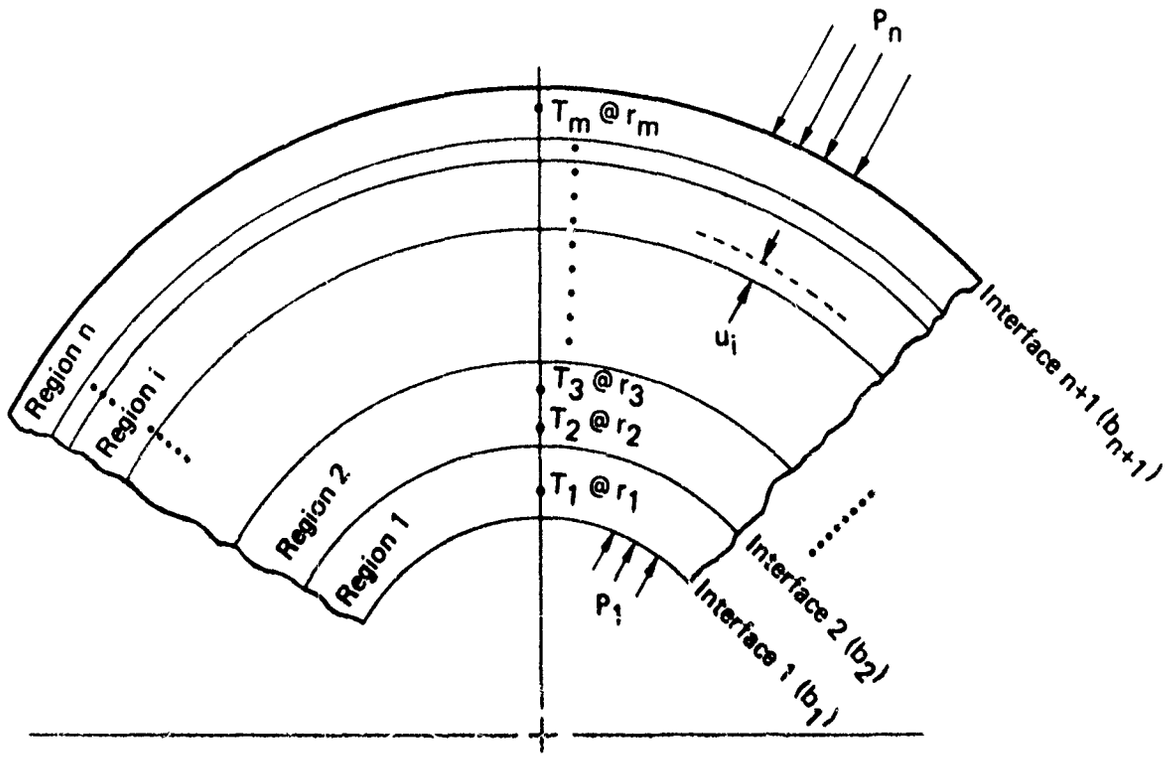

NOTES:

- Total wall thickness ($b_{n+1} - b_1$) is divided into n arbitrarily sized regions, creating n+1 interfaces.
- Temperatures are provided at m arbitrarily spaced radius values and are constant with respect to the axial and circumferential directions.
- Radial displacements from an initial isothermal state occur for each interface, u_i.
- Mechanical properties are assumed constant within regions at values that are temperature averaged with respect to the radial temperature variance.

Fig. 3 Thermal Stress Geometry and Nomenclature

If $T(r)$ is the temperature at radius r and T_0 is the uniform temperature for the cylinder at which no stresses are present then $T = T(r) - T_0$ will define the variable T in the following development.

The radial displacement of any point within the ith region of the cylinder in Fig. 3 due to the temperature gradient T is (from Ref. 10)

$$u_i = \frac{1+\nu}{1-\nu}\,\frac{1}{r}\int_{b_i}^{r}(\alpha T)r\,dr + C_{i,1}\,r + \frac{C_{i,2}}{r}\,. \qquad (28)$$

The radial (r), tangential (θ), and axial (z) stresses are given (respectively) as

$$\sigma_{r_i} = \frac{-E_i}{1-\nu}\,\frac{1}{r^2}\int_{b_i}^{r}(\alpha T)r\,dr + \frac{E_i}{1+\nu}\,\frac{C_{i,1}}{1-2\nu} - \frac{C_{i,2}}{r^2}\,, \qquad (29)$$

$$\sigma_{\theta_i} = \frac{E_i}{1-\nu}\,\frac{1}{r^2}\int_{b_i}^{r}(\alpha T)r\,dr - \frac{(\alpha T)E_i}{1-\nu} +$$

$$\frac{E_i}{1+\nu}\left(\frac{C_{i,1}}{1-2\nu} + \frac{C_{i,2}}{r^2}\right)\,, \quad \text{and} \qquad (30)$$

$$\sigma_{z_i} = -\frac{(\alpha T)E_i}{1-\nu} + \frac{2\nu E_i C_{i,1}}{(1+\nu)(1-2\nu)}\,. \qquad (31)$$

In these equations $C_{i,1}$ and $C_{i,2}$ are constants of integration that apply to the ith region.

Ref. 10. S. Timoshenko and J. N. Goodier, Theory of Elasticity, McGraw-Hill, New York, 1951.

The coefficient of expansion has been brought under the integral sign in writing these equations since it is always permissible to consider αT (the unrestrained strain due to temperature) as a single quantity. As a result α need not be constant over the range of temperature changes.

Since there are n regions, a total of 2n constants of integration must be found. These constants are determined so that equilibrium and compatibility are satisfied on the faces and interfaces of the layers. Equilibrium on the inner and outer faces requires that

$$\sigma_r\Big|_{b_{i+1}} = -p_1 \tag{32}$$

and

$$\sigma_r\Big|_{b_{n+1}} = p_{n+1} \ , \tag{33}$$

where p_1 and p_{n+1} are the pressures on the inner and outer faces. At each of the interfaces the equilibrium condition,

$$\sigma_{r_i}\Big|_{b_{i+1}} = \sigma_{r_{i+1}}\Big|_{b_{i+1}} \ , \quad i = 1 \text{ to } (n-1) \ , \tag{34}$$

and the compatibility condition,

$$u_i\Big|_{b_{i+1}} = u_{i+1}\Big|_{b+1} \ , \quad i = 1 \text{ to } (n-1) \ , \tag{35}$$

must be satisfied. Substituting Eqs. (28) and (29) into Eqs. (32) through (35) gives

$$\left(\frac{1}{1-2\nu}\right) C_{1,1} - \frac{1}{b_1^2} C_{1,2} = -\frac{p_1(1+\nu)}{E_1} \ , \tag{36}$$

$$\left(\frac{1}{1-2\nu}\right) C_{n,1} - \frac{1}{(b_{n+1})^2} C_{n,2} = (1+\nu) \frac{A_n}{(b_{n+1})^2} - \frac{p_{n+1}}{E_n} \quad , \tag{37}$$

$$\left(\frac{1}{1-2\nu}\right) C_{i,1} - \frac{1}{(b_{i+1})^2} C_{i,2} - \frac{E_{i+1}}{E_i(1-2\nu)} C_{i+1,1} +$$

$$\frac{E_{i+1}}{E_i (b_{i+1})^2} C_{i+1,2} = (1+\nu) \frac{A_i}{(b_{i+1})^2} \; ; \; i=1,2,\ldots,(n-1), \tag{38}$$

and

$$C_{i,1} + \frac{1}{b_{i+1}} C_{i,2} - C_{i+1,1} - \frac{1}{(b_{i+1})^2}$$

$$= -(1+\nu) \frac{A_i}{(b_{i+1})^2} \; ; \; i=1,2,\ldots,(n-1) \; , \tag{39}$$

where

$$A_i = \frac{1}{1-\nu} \int_{b_i}^{b_{i+1}} (\alpha T) r \, dr \quad . \tag{40}$$

Solution of the 2n simultaneous equations generated by Eqs. (36) through (40) gives the $C_{i,1}$ and $C_{i,2}$ coefficients. Substitution of these into Eqs. (29) through (31) yields σ_{r_i}, σ_{t_i}, and σ_{z_i} for restrained ends.

The resultant axial force for restrained ends is

$$R = 2\pi \sum_{i=1}^{n} \int_{b_i}^{b_{i+1}} \sigma_{z_i} \, r \, dr \quad ,$$

which, by using Eq. (31), becomes

$$R = -2\pi \sum_{i=1}^{n} \frac{E_i}{i - \nu} \int_{b_i}^{b_{i+1}} (\alpha T) r \, dr - \frac{2\nu E_i C_{i,1}}{(1 + \nu)(1 - 2\nu)} \int_{b_i}^{b_{i+1}} r \, dr \, .$$

From Eq. (40) we find

$$\frac{R}{\pi} = -2 \sum_{i=1}^{n} \left\{ E_i A_i - \frac{\nu E_i C_{i,1}}{(1 + \nu)(1 - 2\nu)} \left[(b_{i+1})^2 - b_i^{\,2} \right] \right\} \, . \quad (41)$$

To determine the axial stresses for unrestrained ends we determine the stresses due to an axial force of -R and superimpose these upon the previously determined stresses. The stresses due to -R can be shown to be

$$\sigma_{z_i} = - \frac{E_i R}{\pi \sum_{j=1}^{n} E_j \left[(b_{j+1})^2 - b_j^{\,2} \right]} \, ; \quad \sigma_\theta = 0; \quad \sigma_r = 0 \, .$$

In the ith region the radial and circumferential stresses for unrestrained ends are then given by Eqs. (29) and (30). The axial stress is

$$\sigma_{z_i} = - \frac{\alpha T E_i}{1 - \nu} + \frac{2\nu E_i C_{i,1}}{(1 + \nu)(1 - 2\nu)} + \frac{E_i (R/\pi)}{\sum_{j=1}^{n} E_j \left[(b_{j+1})^2 - b_j^{\,2} \right]} \, . \quad (42)$$

The thermal stresses as developed here are used in the URLIM program to evaluate the thermal stress failure levels of

radomes. An obvious further assumption is that the region of critical stress in the radome behaves like the cylinder modeled here. Studies by others (Ref. 11) have shown that if the point of interest on the radome is sufficiently far from the nose region, then the cylindrical assumption is sufficiently accurate (i.e., less than 10% error). It is worth noting that the radial dimensions that compare between the cylinder and the radome should be made along the local normal to the radome profile and not along the radius of revolution of the radome profile.

BORESIGHT ERRORS

The prediction of boresight error rates for radar transmission through streamlined radomes is regrettably imprecise. This situation is due in large part to the number of significant variables involved, such as radar frequency, antenna design, antenna placement within the radome and incidence angle variations, radome shape, the magnitude and temperature dependence of the radome dielectric constant, and the transmission loss of the material. Theoretical prediction techniques that are sufficiently general and complete are consequently quite complicated. To add to the confusion, the prediction techniques often do not correlate well with observed data (c.f. Section 8 of Ref. 12). Therefore, the philosophy of the radome error prediction method used here is based on experimental radome data. Interpolation of the available data is made to determine the empirical equation that describes the effects of antenna aperture size, dielectric constant, wall thickness, and wavelength changes on a theoretically perfect room-temperature radome design. An attempt is also made to include the effects of missile dynamics on error slope requirements by averaging the experimental radome error over a fixed 20° gimbal period. Before a discussion of the boresight error analysis is given, a brief account of the radar power loss due to transmission through a radome will be given.

Transmission Losses

A radome must pass electromagnetic radiation efficiently. A reduction of radome transmission efficiency degrades the overall range product or effective noise figure of an airborne radar. Definition of a radome limit from transmission loss requires

---

Ref. 11. R. M. Rivello, "Comparisons of Radome Stress Solutions," APL/JHU EM-3989, August 1965.

Ref. 12. L. B. Weckesser et al., "Environmental Limitations of Alumina, Fused Silica, and Pyroceram 9606 Radomes," APL/JHU TG 865, May 1967.

knowledge of target size and missile-target space geometries. The limitation of a radome from a transmission loss analysis is very vague since transmission losses simply reduce acquisition range. It is conceivable that very large transmission losses (2 to 3 dB) could be tolerated during a homing mission and not degrade target intercept. An increase in radome transmission losses is caused by three phenomena:

1. A change in electrical thickness that produces a reflection loss,

2. An increase in the loss tangent of the radome material that produces an absorption loss, and

3. Distortion of the antenna aperture illumination that changes the antenna gain (this change may produce a gain rather than a loss).

Laboratory experiments at room temperature on a Pyroceram C-band radome verified that reflection losses were less than 1 dB over a 10% frequency bandwidth. The ratios of the square roots of the dielectric constants of Pyroceram to alumina and to fused silica are 0.76 and 1.31, respectively. Using these ratios, 1-dB loss bandwidths for alumina and fused silica are estimated to be 7.6% and 13%, respectively. Thus, reflection losses are less than 1 dB for relative radome design changes of less than 3.8%, 5%, and 6.5% for alumina, Pyroceram, and fused silica, respectively. Also, it has been found that absorption loss (in dB) of a half-wave radome (normal incidence) for loss tangents (tan δ) of less than 0.5 can be approximated by 13.65 tan δ. This expression indicates that tan δ can be as high as 0.05 before 0.7 dB of absorption loss is realized. Therefore, in this study we may safely assume that radome transmission losses will have little influence on the electrical limitations.

Angular Error Prediction Method

An analytical method was developed for predicting the radome angular error slope (e) during flight. This method is based on well-known mathematical relations and experimentally determined constants. The experimental and mathematical characteristics assumed for the radome model are listed below:

1. The radome has a von Karman shape with a length-to-diameter ratio of 2.1.

2. The antenna is an 11-in.-diameter, four-quadrant array with an effective phase-center separation of 3.89 in.

3. The RF bandwidth is zero; i.e., single-frequency operation.

4. The radome has been corrected to have zero error slope at room temperature.

5. The basic thickness of the corrected radome in wavelengths is

$$\frac{d_0}{\lambda_0} = \left(2\sqrt{\varepsilon_0 - \sin^2\beta}\right)^{-1} \quad , \tag{43}$$

where

$$\beta = \tan^{-1}\sqrt{\varepsilon_0} = \text{Brewster's Angle},$$

and

d_0 is the room temperature radome wall thickness,

λ_0 is the center design, free-space wavelength of incident radar, and

ε_0 is the room temperature dielectric constant.

6. The worst-case average error slope occurs in the gimbal region through the radome nose and is linear between ±10°. This average error slope is derived from experimental data by averaging the worst-case angular error over ±10°; i.e.,

$$\frac{\varepsilon_{max}}{20^\circ} = \Delta e \quad .$$

7. The worst-case angular error slopes are associated with polarizations parallel to the plane of rotation; i.e., the E-plane.

8. Radome transmission losses resulting in lower receiver sensitivity do not degrade missile homing performance.

9. A change in electrical thickness is directly related to a change in angular error slope; i.e.,

$$\frac{\Delta e}{e_0} = C_1 \frac{\Delta \psi}{\psi_0} \quad ,$$

where

$$\psi = 2\pi \frac{d}{\lambda} \sqrt{\epsilon_0 - \sin \phi}$$

(ψ is the electrical thickness of the radome; ϕ is the radar incidence angle).

Laboratory measurements at C, X, and K bands have indicated that angular error magnitudes are approximately inversely proportional to the antenna diameter in wavelengths or to interferometer gain. Also, other laboratory investigations with a low-dielectric-constant radome sandwich design have been made (Ref. 13) and the results indicate that angular errors are generally lower over a broadened frequency band for materials of lower dielectric constant. In particular, data obtained on a C-band Pyroceram radome and a two-ply sandwich wall radome indicated that the improvement in frequency bandwidth is approximately proportional to the ratio of the square roots of the dielectric constants of the two radome designs. A mathematical expression describing these results is

$$\frac{\Delta e}{e_0} \approx \frac{(\text{Dielectric Constant Function})^{\frac{1}{2}}}{(\text{Interferometer Gain})} \frac{\Delta \psi}{\psi_0} \quad ,$$

Ref. 13. R. H. Hallendorff, "Wideband Radome Antenna Research," Section 3/9, "Research and Development Quarterly Report," APL/JHU U-RQR/64-3, July-September 1964.

which can be written as

$$\frac{\Delta e}{e_0} = \frac{A\sqrt{\varepsilon_0 - 1}}{\frac{4\pi}{\lambda_0}\frac{D}{2}} \frac{\Delta\psi}{\psi_0} , \tag{44a}$$

or

$$\Delta e = \frac{B\sqrt{\varepsilon_0 - 1}}{\frac{D}{2\lambda_0}} \frac{\Delta\psi}{\psi_0} , \tag{44b}$$

where D is the antenna diameter and $B = Ae_0/4\pi$. The ε_0 term in the numerator of Eq. (44a) is included for converging the error magnitude to zero for the case of a radome material having a relative dielectric constant of 1. The constant B in Eq. (44b) was determined empirically from error slope data taken at C-, X-, and K-band frequencies on Pyroceram radomes. Experimental average angular error slopes occurring through the radome nose were determined as a function of frequency and plotted as a function of percent change in frequency ($\Delta f/f_0$). The center frequency (f_0) is defined as the frequency where the error slope through the nose equals zero.

Figures 4, 5, and 6 show the typical change in experimental average error slope through the nose as a function of percent change in frequency for a constant-wall half-wave radome. The K-band data of error slope versus frequency change shown in Fig. 5 are estimated from boresight error measurements that were made on a full-wave (two half-wave thicknesses) and a third-order (three half-wave thicknesses) radome using a pair of standard-gain horns with a gain approximately 10 dB down from that expected from an 11-in.-diameter antenna. Also shown in these figures are straight line approximations to the experimental data. The slopes of the experimental functions generated in Figs. 4 and 5 are shown to be equal to:

$$|\text{slope}| = \left|\frac{\Delta e}{\Delta f/f_0}\right| \quad \text{or} \quad \frac{\Delta e}{\Delta\psi/\psi_0} = \frac{B\sqrt{\varepsilon_0 - 1}}{\frac{D}{2\lambda_0}} . \tag{45}$$

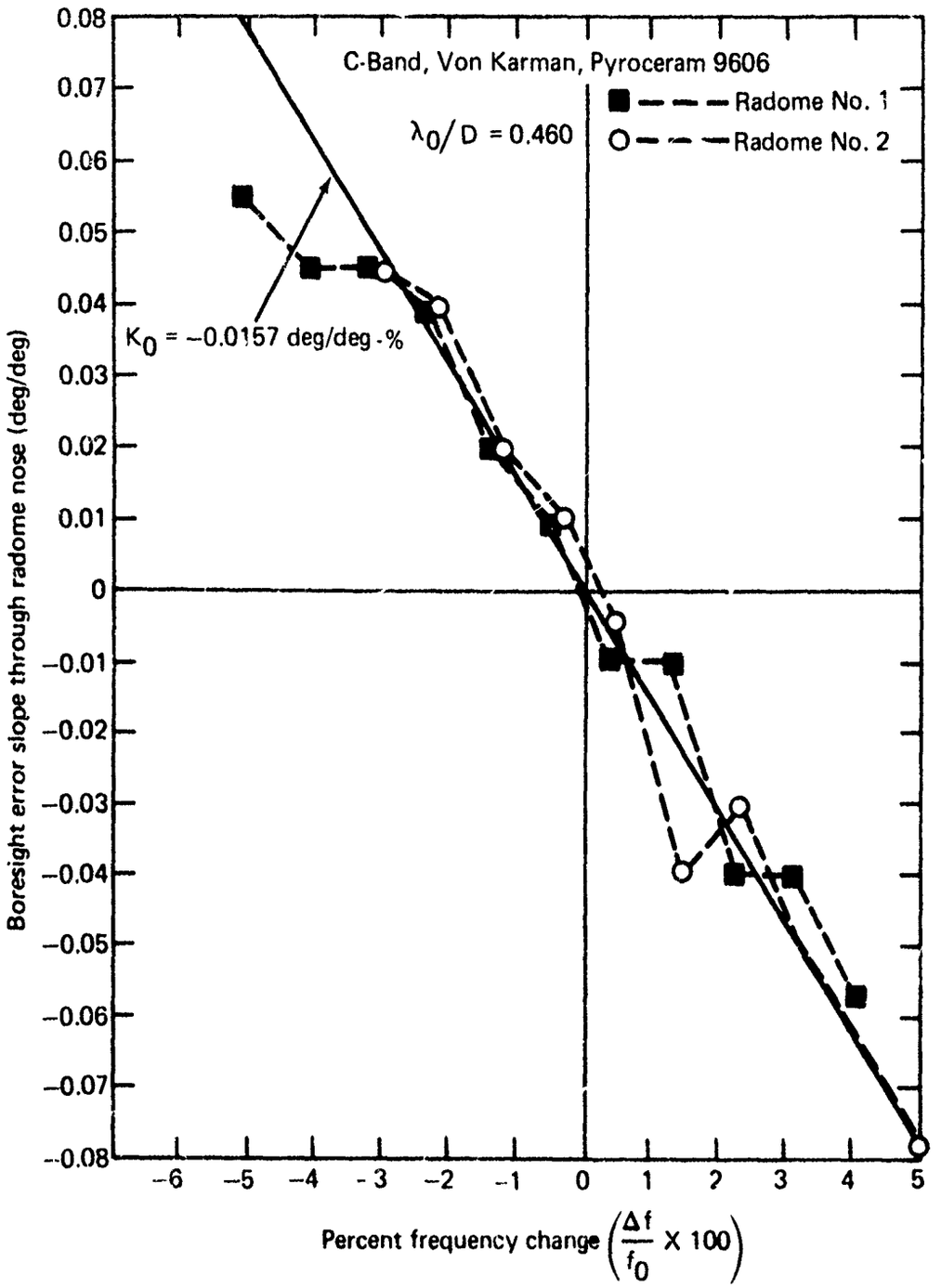

Fig. 4 C-Band Boresight Error Slope versus Percent Frequency Change

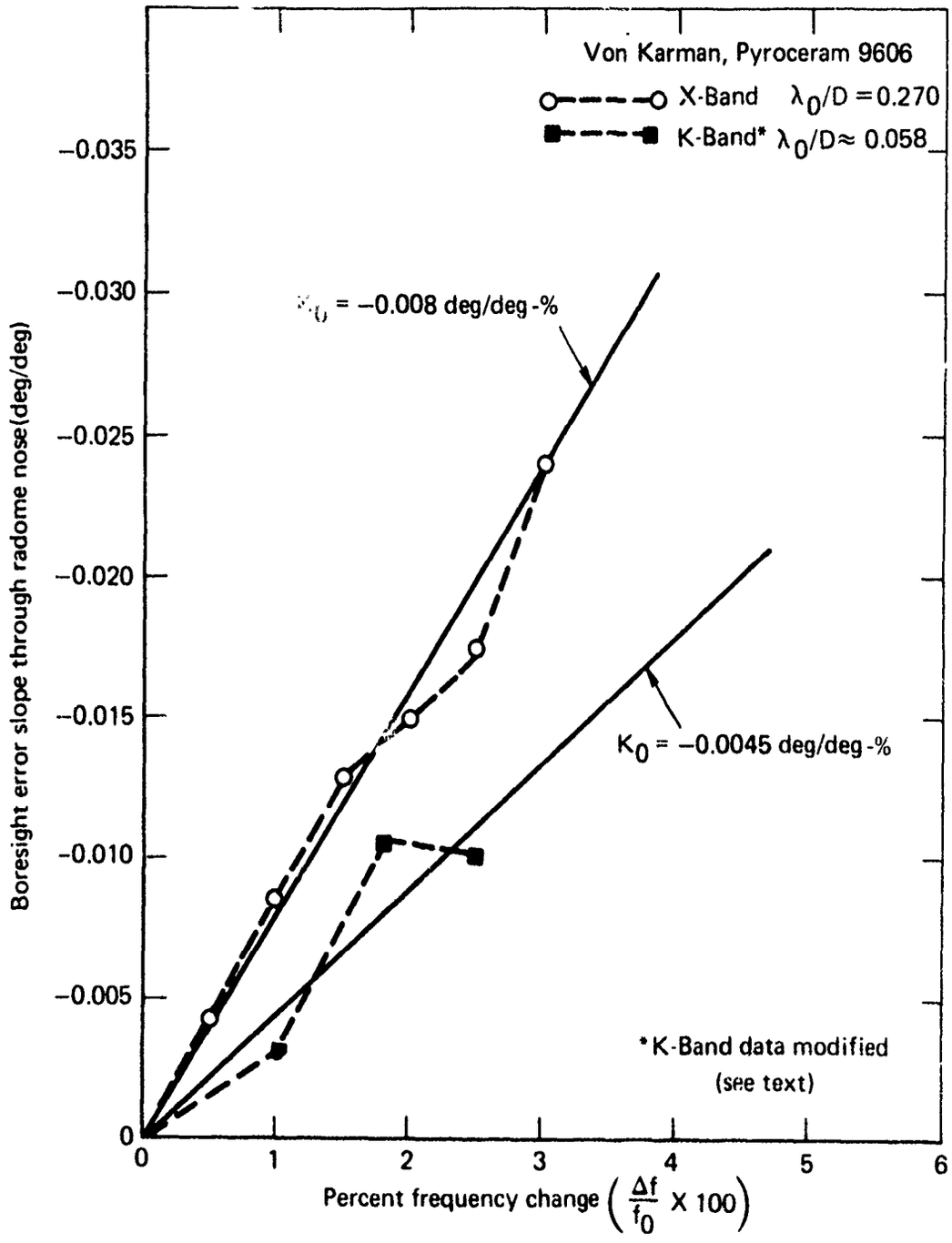

Fig. 5 X-and K-Band Boresight Error Slope versus Percent Frequency Change

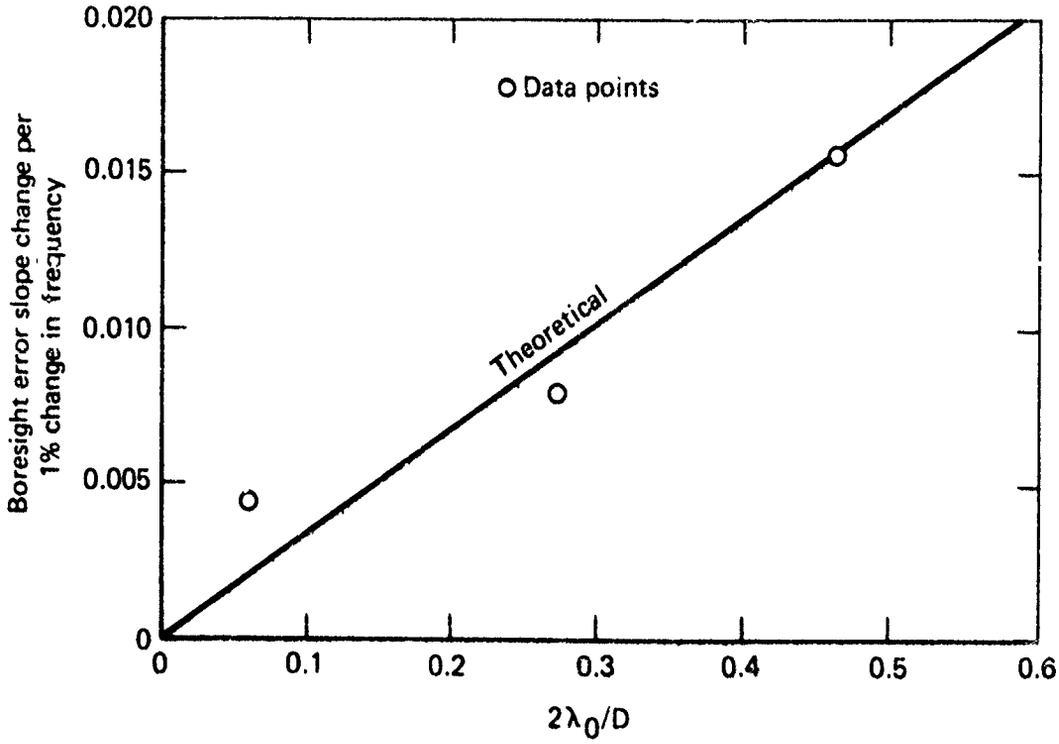

Fig. 6 Comparison of Error Slope Magnitude versus Reciprocal of Antenna Aperture Size in Wavelengths $(2\lambda_0/D)^{-1}$ (Pyroceram 9606)

The numerical expression derived from experimental data for use in the radome analysis is

$$\Delta e = 1.615\ \lambda_0 \frac{\sqrt{\epsilon_0 - 1}}{a} \frac{\Delta\psi}{\psi_0} \text{ deg/deg} \quad , \tag{46}$$

where a = D/2. An increase in error slope (Δe) can be determined from Eq. (46) for a given change in electrical thickness ($\Delta\psi/\psi_0$) once the frequency (wavelength), relative dielectric constant, and effective phase center separation (a) are known.

What remains now is to calculate $\Delta\psi/\psi_0$ for the radome wall as a function of trajectory time. To do this the wall is assumed to be divided into m subsections through the thickness. Any single section (n) is considered to have its own value of electrical thickness (ψ_n):

$$\psi_n = \frac{2\pi d_n}{\lambda} \sqrt{\epsilon_n - \sin^2\phi} \quad , \tag{47}$$

and the average electrical thickness of the whole wall is:

$$\psi_{avg} = \frac{1}{m} \sum_{n=1}^{m} \psi_n \quad . \tag{48}$$

The relative electrical thickness change is then

$$\frac{\Delta\psi}{\psi_0} = \frac{\psi_{avg} - \psi_0}{\psi_0} = \frac{\psi_{avg}}{\psi_0} - 1$$

$$= \sum_{n=1}^{n=m} \left[\frac{\sqrt{\epsilon_0 + \Delta\epsilon_n - \sin^2\phi}}{\epsilon_0 - \sin^2\phi} \left(\frac{1}{m} + \frac{\Delta d_n}{d_0} \right) \right] - 1 \quad . \tag{49}$$

In the URLIM program the electrical thickness change (Eq. (49)) is calculated using the same wall thickness divisions used for the thermal stress analysis in subroutine SIGMET. The result is made available to routine MOBSER where Eq. (46) is solved for the boresight error.

AERODYNAMIC LOAD

During the flight of a missile, considerable aerodynamic pressure and skin friction can develop on the radome because of its high speed and angle of attack. Also, during maneuvering to the target, high lateral and angular accelerations can be developed, causing inertial forces in the radome structure. Calculating the magnitude of these forces and the resultant stresses is important in radome design in order to determine the limitations of the radome and hence the missile. The calculation procedure is designed to be applied at all times during the flight of the missile. Moreover, if the calculations are done over a variety of trajectories that cover the missile's propulsion capabilities, then the mechanical load limits for the radome can be accurately stated.

The present analysis of mechanical loads on a radome considers forces caused by axial and normal pressure drag, axial friction drag, normal (or lateral) and axial accelerations, and angular accelerations. Figure 7 is a schematic of a radome with the various forces listed that can act at any time during a flight. F_{Nr} and F_{Ar} are the normal and axial aerodynamic forces acting on the radome and are shown acting at the radome's center of pressure (cp). The inertial forces are shown acting at the center of mass of the radome, m_r. The sum of these forces can be resolved into forces and moments acting at the base of the radome (point O, Fig. 7). These forces in turn cause stresses in the walls of the radome that can be calculated from knowledge of the radome's base radius (RB) and wall thickness (t).

Figure 7 is a schematic of a radome during flight with three coordinate systems. Coordinate system X',Y' is inertial and fixed to the earth; system X,Y is centered at the center of mass of the missile and is aligned at any instant with the flight path (i.e., X is along the velocity vector and Y is perpendicular to it). Lateral maneuvers are considered to be along the Y-axis. The third coordinate system (x,y) is located at the radome's base and is fixed to the missile body; i.e., it is aligned with the missile axes, x along the centerline and y perpendicular to the centerline at O. All directions shown in Fig. 7 are positive.

X',Y' – Coordinate system attached to ground

X,Y – Coordinate system along and perpendicular to velocity vector of missile at center of mass of missile

x,y – Missile body coordinate system located at base of radome ("O")

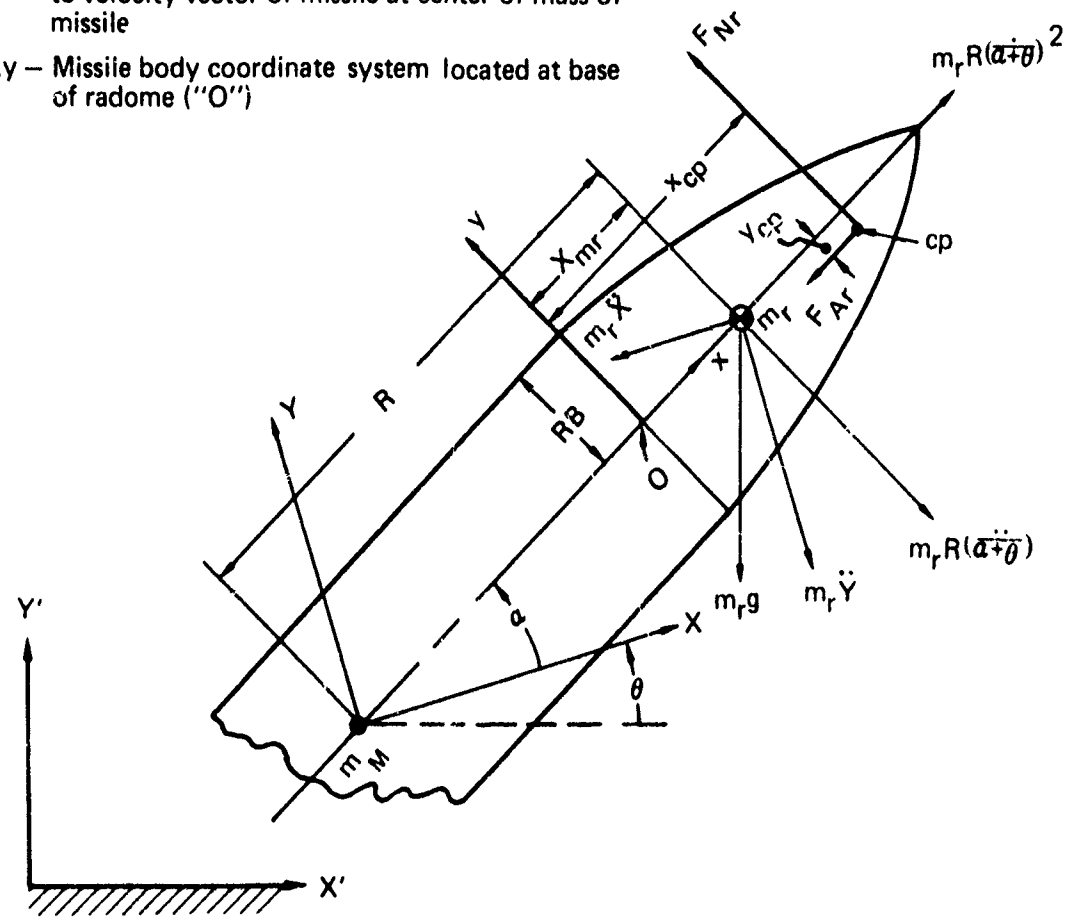

Fig. 7 Coordinate System and Forces for Radome Mechanical Load Analysis

During the flight, the aerodynamic pressure and friction forces act on the radome with a magnitude and direction that is dependent on speed (Mach number) and angle of attack (α). For various shapes, these forces are tabulated in coefficient form and are divided into axial (x-direction) and normal (y-direction) components, as

$$C_{Nr} = \frac{F_{Nr}}{(\gamma_0 p_0 M_0^2/2)A} \quad , \tag{50a}$$

and

$$C_{Ar} = \frac{F_{Ar}}{(\gamma_0 p_0 M_0^2/2)A} \quad , \tag{50b}$$

where C_{Ar} and C_{Nr} are the force coefficients for the radome in the axial and normal directions; $\gamma_0 p_0 M_0^2/2$ is the dynamic pressure of the stream with static condition or pressure p_0, velocity (Mach number) M_0, and specific heat ratio γ_0; and A is the area of the base of the radome. These component pressure forces are said to act at the center of pressure (cp) where their effect on the radome is resolved into the component forces with no moment. The location of this point itself depends on Mach number and angle of attack and may be positioned away from the body centerline. As shown in Fig. 7, the location of the center of pressure is defined by x_{cp} and y_{cp}. Reference 14 is an excellent source for these coefficients for several nosecap shapes. For the present analysis, the center of pressure is assumed to vary only along the x-axis and to have no displacement from the centerline (i.e., $y_{cp} = 0$).

During an engagement, the missile's control system will require rapid changes in the flight path direction. To accomplish this, the missile will change its angle of attack to provide sufficient lift for the maneuver. The present analysis considers only lateral accelerations caused by angle of attack changes in the X,Y plane. At some angle of attack during a maneuver, the rate of change of angle of attack may be quite large. Dynamic simulations of various missile configurations are available to supply these values. The causes of inertial forces that can be considered to be acting at the center of mass of the radome are

---

Ref. 14. E. T. Marley and H. Ginsberg, "Supersonic Pressure Distribution and Axial Force Characteristics of Axisymmetric Noses at Angle of Attack," Paper Presented at the Seventh U.S. Navy Symposium on Aeroballistics, 7-9 June 1965.

Lateral acceleration: $m_r\ddot{Y}$,

Axial acceleration: $m_r\ddot{X}$,

Angular velocity: $m_r R\left(\dot{\alpha + \theta}\right)^2$,

Angular acceleration: $m_r R\left(\ddot{\alpha + \theta}\right)$, and

Radome mass: $m_r g$.

These forces are shown in Fig. 1 acting in positive directions.

The resultant forces at the base of the radome and moment about point 0 are found to be

$$F_x = F_{Ar} + m_r\left[g \sin(\alpha + \theta) + \ddot{X}\cos\alpha + \ddot{Y}\sin\alpha - R\left(\dot{\alpha + \theta}\right)^2\right], \tag{51a}$$

$$F_y = -F_{Nr} + m_r\left[g\cos(\alpha + \theta) - \ddot{X}\sin\alpha + \ddot{Y}\cos\alpha + R\left(\ddot{\alpha + \theta}\right)\right], \tag{51b}$$

$$M_0 = -F_{Nr}\,x_{cp} + m_r x_{mr}\left[g\cos(\alpha + \theta) - \ddot{X}\sin\alpha + \ddot{Y}\cos\alpha + R\left(\ddot{\alpha + \theta}\right)^2\right], \tag{51c}$$

These stresses caused by the forces are distributed around the base of the radome and are maximum either at the top (y=RB) or at the bottom (y=-RB) or the radome's base. These stresses are

$$\sigma_{y=RB} = \frac{M_0}{\pi(RB)^2 t} - \frac{F_x}{2\pi(RB)t}, \quad \text{and} \tag{52a}$$

$$\sigma_{y=-RB} = \frac{-M_0}{\pi(RB)^2 t} - \frac{F_x}{2\pi(RB)t}. \tag{52b}$$

The angle of the missile's velocity vector with the local horizongal (θ) is often called the quadrant elevation. It is determined from the trajectory information input by the user, namely the altitude and velocity as functions of time. In the brief derivations that follow it will be assumed that the altitude and velocity are known at two points along the trajectory; i.e., Z_1 and V_1 are known at t_1, and Z_2 and V_2 at t_2. Further, it is assumed that the vertical acceleration of the missile ($\ddot{Z}$) is constant during the time interval $t_2 - t_1$ and that the quadrant elevation does not change (i.e., $\theta_1 = \theta_2 = \theta$). If $\ddot{Z}$ is constant, then

$$\ddot{Z} = C_1 \ ,$$

$$\dot{Z} = C_1 t + C_2 \ ,$$

and

$$Z = (C_1/2)t^2 + C_2 t + C_3 \ .$$

At the two times t_1 and t_2, four relationships may be written:

$$\dot{Z}_1 = V_1 \sin\theta = C_1 t_1 + C_2 \ , \tag{53a}$$

$$\dot{Z}_2 = V_2 \sin\theta = C_1 t_2 + C_2 \ , \tag{53b}$$

$$Z_2 = (C_1/2)t_2^2 + C_2 t_2 + C_3 \ , \quad \text{and} \tag{53c}$$

$$Z_1 = (C_1/2)t_1^2 + C_2 t_1 + C_3 \ . \tag{53d}$$

Equation (53a) may be rewritten as

$$C_2 = V_1 \sin\theta - C_1 t_1 \ , \tag{53a1}$$

and substitution into Eq. (53b) gives

$$V_2 \sin\theta = C_1 t_2 + V_1 \sin\theta - C_1 t_1 \ . \tag{53b1}$$

If we assume $t_1 = 0$, so that t_2 will now represent the time interval between points 1 and 2 then Eq. (53d) becomes

$$C_3 = Z_1 \ , \tag{53d1}$$

Eq. (53b1) becomes

$$V_2 \sin\theta = C_1 t_2 + V_1 \sin\theta \ , \tag{53b2}$$

and Eq. (53c) becomes

$$Z_2 = \frac{C_1}{2} t_2^{\,2} + (V_1 \sin\theta) t_2 + Z_1 \ . \tag{53c1}$$

Equation (53b2) may be rewritten as:

$$C_1 = (V_2 - V_1)(\sin\theta)/t_2 \ . \tag{53b3}$$

Substitution of Eq. (53b3) into Eq. (53c1) gives

$$\theta = \sin^{-1} \frac{2(Z_2 - Z_1)}{t_2(V_2 + V_1)} \ . \tag{54}$$

The solutions to Eqs. (51a), (51b), (51c), (52a), and (52b) are obtained by the use of Eq. (54) in the AERLOAD subroutine and provide attachment stresses as a function of trajectory time in the URLIM program.

2. NUMERICAL METHODS

TRANSIENT HEAT CONDUCTION

Consider a body divided into N mass lumps (nodes) as shown below:

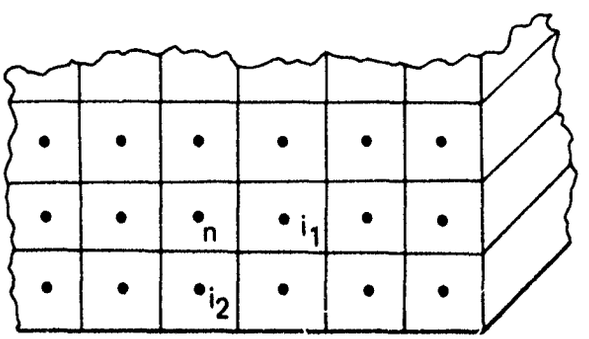

In general, any node n may be connected thermally to any number of other nodes. To determine the temperature of any node (T'_n) due to Fourier conduction within the material at some time interval away from an initial starting time, the following equation is solved for T'_n:

$$\frac{\rho V_n c_p (T'_n - T_n)}{(t' - t)} = -\left[\sum_{i=1}^{K} \frac{k_{n-i} A_{n-i}}{L_{n-i}} (T_n - T_i)\right], \qquad (55)$$

where

ρ is the density of the material,

V_n is the volume of the node,

c_p is the specific heat of the material,

t is time (t being the current time and t' being the time in the future),

k_{n-i} is the thermal conductivity between n and each connecting node i,

A_{n-i} is the area perpendicular to heat flow between n and each connecting node i,

L_{n-i} is the distance between n and the connecting nodes i, perpendicular to A,

T is temperature (T' being at t', T being at t), and

K is the total number of directly connecting nodes.

The left-hand side of Eq. (55) represents the change in internal energy of the node n during the time interval $t' - t$. The right-hand term of Eq. (55) is the net heat transferred to or from the node by all the nodes it is in contact with. Equation (55) is, moreover, the finite difference approximation to Eq. (4a) derived earlier in this volume (Chapter 4 of Ref. 15 also contains this derivation). The right-hand side of Eq. (55) can have additional terms which include other modes of heat transfer between nodes as well as the application of boundary conditions for external surface nodes. The equations listed below define how these additional modes of heat transfer are calculated within the program.

Radiation Term

$$\dot{q}_R = \sigma \sum_{i=1}^{R} F_{n-i} A_{n-i} \epsilon_{n-i} \left(T_n^4 - T_i^4 \right) ,$$

where

σ is the Stefan-Boltzman constant,

F_{n-i} is the view factor from n to i,

Ref. 15. G. M. Dusinberre, Heat-Transfer Calculations by Finite Differences, International Textbook Co., Scranton, PA, 1961.

ε_{n-i} is the infrared emissivity factor from n to i, and

R is the total number of nodes radiating with node n.

Constant Flux Terms

$$q'' = \sum_{i=1}^{Q''} \dot{q}''_{n-1} A_{n-1} ,$$

where:

$\dot{q}''_{n-i}$ is the independently specified flux between n and the independent source i per unit area, and

Q'' is the number of independent sources.

Convective Flux

Convective (aerodynamic) heating is a boundary condition that is solved for implicitly by the SAERO subroutine and therefore does not enter into the nodal temperature solution being described here. Convective flux boundary conditions can be specified by the user on as many surfaces of the thermal model as are desired.

Internal Generation

$$\dot{q}'''_n = f(t) ,$$

where

$\dot{q}'''_n$ is the heat generated within node n due to independent phenomena (e.g., nuclear fission, Joule heating, chemical reaction, Peltier effect, etc.), which may be time dependent.

Solution Technique

The transient solution for N nodal temperatures requires choosing a time step $(t' - t)$ and solving the N equations of the form of Eq. (55) for all values of T'_n. The N temperatures are stored in the subscripted variable $\underline{T}$ (dimensioned from 1 to N); each right-hand side of Eq. (55) is combined into the subscripted

variable $\overline{Q}$ (dimensioned from 1 to N), and each $\rho V_n c_p$ is stored in the subscripted variable $\overline{C}$ (dimensioned from 1 to N). The N equations are then reduced to:

$$\overline{T}' = \overline{T} - (\overline{Q}/\overline{C}) \quad (t' - t) \ , \tag{56}$$

where the bar indicates a vector of dimension N.

For completeness, and to appreciate the nonlinearity of Eq. (55) or (56), it is noted that the coefficients in these equations are dependent on the temperature of the node; i.e., k, ε, and c_p are treated as functions of temperature. If $k = f(T)$ in general, then for Eq. (55):

$$k_{n-i} = f\left(\frac{T_n + T_i}{2}\right) \ , \tag{57}$$

and if $\varepsilon = g(T)$ in general, then

$$\varepsilon_{n-i} = g\left(\frac{T_n + T_i}{2}\right) . \tag{58}$$

The special case of two nodes of differing materials (hence different k functions) connected together through a contact resistance is handled by the COMCON subroutine, which evaluates the following equation:

$$\dot{q}_{cc} = \sum_{i=1}^{C} K_{cc} \ (T_n - T_i) \ , \tag{59}$$

where

$$\frac{1}{K_{cc}} = \frac{1}{(k_n A/L)\Big|_{n-x}} + \frac{1}{k_2} + \frac{1}{(k_i A/L)\Big|_{x-i}} \ . \tag{59a}$$

Subscript x denotes the location of the interface between nodes n and i, and

$$k_n = f_1\left(\frac{T_n + T_x}{2}\right) ,$$

$k_2 = f_2(T_x)$, the thermal conductance of the contact, and

$$k_i = f_3\left(\frac{T_x + T_i}{2}\right) .$$

Implied in Eq. (59) is a solution for T_x that is carried out by subroutine COMCON and is based on the fact that the interface has no thermal capacity (therefore all the heat conducted to one side of the contact is completely conducted out at the other side).

The transient solution is obtained by choosing a time step $(t' - t)$ and solving all N equations of the form of Eq. (56) for T'. One must be careful in choosing the time step so that the solution will be numerically stable. The rule for choosing a time step is

$$\Delta t = 0.9\left[\underset{n=1,N}{\text{MIN}}\left(\frac{C_n}{\sum_{i=i}^{k} H_{n-i}}\right)\right] , \tag{60}$$

where H_{n-i} is the net conductance between nodes n and i and can be composed of conduction and/or radiation terms:

$$H_{n-i} = \frac{k_{n-i} A_{n-i}}{L_{n-i}} + \sigma(\varepsilon FA)_{n-i}\left(T_i + T_n\right)\left(T_i^2 + T_n^2\right) .$$

MIN( ) represents a choice of the minimum value of all N such values. (The N values of ΣH_{n-i} are stored in the vector $\overline{H}$ within the computer program.) Equation (60) can be viewed as a

statement of the second law of thermodynamics; that is, for the node in the network with the combination of smallest thermal capacity (C_n) and the largest total thermal conductance (ΣH_{n-i}), the amount of heat that would flow out of the node during Δt if all surrounding nodes were at 0°R would not cause the temperature of that node to be less than 0°R. Algebraically, the relationship can be seen by letting T_i and T'_n approach 0 in Eq. (55). In Eq. (60) we have arbitrarily taken 90% of this minimum to ensure stability.

In the computer program, the STEP routine computes Δt and the nodal temperatures via Eqs. (60) and (56), respectively.

Orthogonal Geometries

The fundamental heat conduction equation was described in Section 1 of this report. In those discussions, the spatial coordinate system used in the partial differential equations was required to be orthogonal. When the partial differential equations are approximated by difference equations (e.g., Eq. (55)) proper care should be exercised to see that the nodal network (i.e., the geometry) is orthogonal. In Eq. (55), orthogonality is incorporated in the two terms A_{n-i} and L_{n-i}, where A is a "contact" area between adjacent nodes, and L is the distance perpendicular to A between node centers. In coordinate systems with natural curvature (cylindrical and spherical, for example) the simple A/L approximation is not correct because the effects of curvature are ignored. In the following derivatives, the partial differential equations will be written and the characteristic solutions for steady state will be obtained for two adjacent nodes. The appropriate correction terms will then be identified.

Cylindrical Nodes

Considering heat conducted in the radial direction only in the steady state, the Fourier heat equation (c.f. Eq. (2)) is written as

$$\frac{\partial^2 T}{\partial r^2} + \frac{1}{r}\frac{\partial T}{\partial r} = 0 \quad .$$

If $p = dT/dr$, then by substitution and allowing the partial derivatives to be total derivatives,

$$dp/dr + p/r = 0 \quad .$$

Further, if p is of the form $p = dT/dr = C/r$, then

$$T(r) = C \ln r + D ,$$

where C and D are constants to be determined by the boundary conditions depicted in the following sketch:

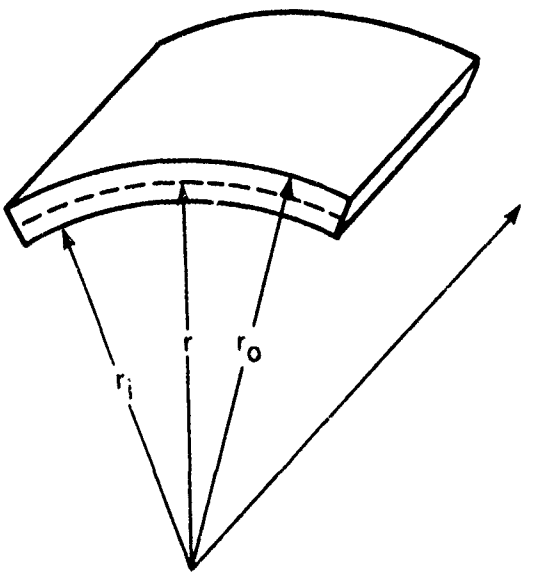

In the sketch the nodal interface is at r, the inner node center is at r_i with temperature T_i, and the outer node center is at r_o with temperature T_o. Using these two conditions in the above equation for $T(r)$ will yield:

$$T(r) = T_o + \frac{(T_o - T_i)}{\ln (r_o/r_i)} (\ln r - \ln r_o) .$$

The heat conducted through the nodal contact is given by

$$\dot{q}(r) = -A(r)\, k\, \overline{\nabla} T ,$$

where $\bar{\nabla}$ is the gradient operator (c.f. Eq. (6)) and reduces to dT/dr in this unidirectional case. A(r), the function relating cross-sectional area to radius, for the nodes shown is

$$A(r) = (\theta_1 - \theta_2)rz \quad ,$$

where z is the depth or axial dimension, and θ_1 and θ_2 are the angular locations of the node centers. When the above relationships for A(r) and T(r) are substituted in the equation for q(r) the following equation results:

$$q(r) = \frac{-z\,(\theta_1 - \theta_2)\,k(T_o - T_i)}{\ln\,(r_o/r_i)} \quad .$$

Comparing this equation with Eq. (55) will reveal that if

$$\frac{A_{n-i}}{L_{n-i}} = \frac{(\theta_1 - \theta_2)\,z}{\ln\,(r_o/r_i)} \quad ,$$

then proper consideration for the cylindrical curvature will have been made. The curvature effect derives from the cross-sectional area having a dependence on the coordinate perpendicular to the area. In cases where the area is invariant in the direction of heat flow (rectilinear coordinates, for example) no "correction" term will be required.

For conduction in the circumferential direction in a cylinder (i.e., in the θ direction), the following partial differential equation is written:

$$\frac{1}{r^2}\,\frac{\partial^2 T(\theta)}{\partial\,\theta^2} = 0 \quad ,$$

which simplifies to

$$dT/d\theta = C \quad ,$$

or

$$T(\theta) = C\theta + D \quad ,$$

where C and D are again constants of integration determined by the boundary conditions sketched in the following figure:

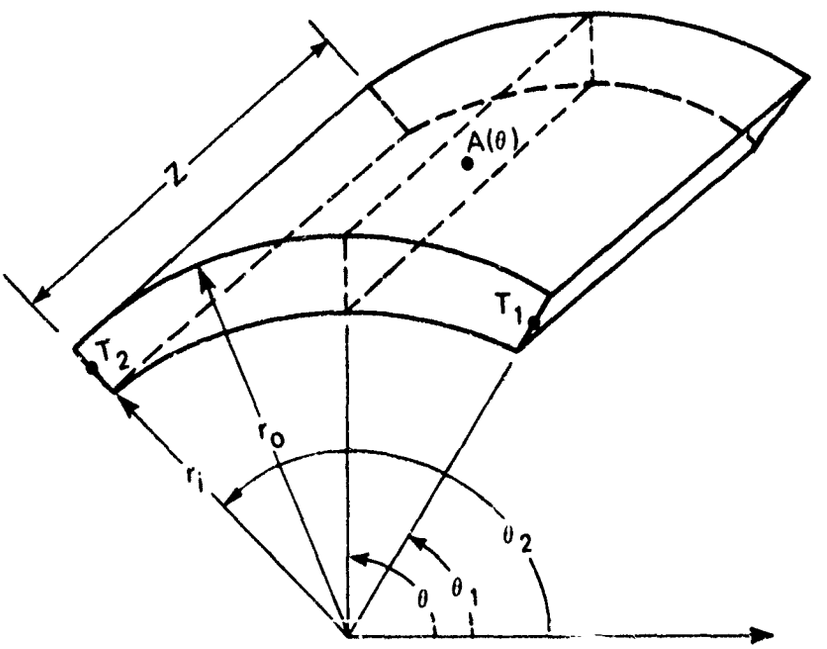

The heat conducted circumferentially between the nodes in the sketch is given by

$$\dot{q}(\theta) = A(\theta)\, k\, \frac{1}{r}\, \frac{\partial T}{\partial \theta} \quad ,$$

with

$$A(\theta) = z\,(r_o - r_i) \quad ,$$

hence

$$\dot{q}(\theta) = \frac{(r_o - r_i)\, z\, [T(\theta_2) - T(\theta_1)]\, k}{r\,(\theta_2 - \theta_1)} \quad ,$$

where r is the average radius, or the radius of the node centers; i.e.,

$$r = (r_o + r_i)/2 \quad .$$

In this case the term $(r_o - r_i)z$ is the cross-sectional area and $r(\theta_2 - \theta_1)$ is the path length between node centers and there is no correction term. This is as expected because there is no variance of the area normal to the circumferential direction. By a similar argument, the axial cylindrical direction will have no correction term associated with it.

Spherical Nodes

In spherical geometries the coordinate system consists of (a) the co-latitudinal angle (ϕ) measured from the pole of the sphere with positive radial values (i.e., the "North" pole); (2) the longitudinal angle (θ) measured as projections in the equatorial plane; and (c) the radial distance (r) measured from the center of the sphere. In the nodal sketches that follow, these directions will be illustrated for clarity.

Considering only conduction in the co-latitudinal direction at steady state, the Fourier equation is

$$d^2T/d\phi^2 + \text{ctn } \phi \; dT/d\phi = 0 \quad .$$

If we let $dT/d\phi = p = C \csc \phi$, then

$$dp/d\phi + \text{ctn } \phi \; p = 0 \; , \tag{61}$$

by substitution. Also,

$$dp/d\phi = -C \csc \phi \; \text{ctn } \phi \quad ,$$

so that by substitution in Eq. (61),

$$-\csc \phi \; \text{ctn } \phi + \text{ctn } \phi \; \csc \phi = 0 \; ,$$

which is an identity and verifies the choice of $p = C \csc \phi$. Hence,

$$dT/d\phi = C \csc \phi \ ,$$

and

$$T(\phi) = C \ln (\tan \phi/2) + D \ ,$$

where C and D are integration constants determined by the boundary conditions described next. The sketch below shows two spherical nodes emphasizing the co-latitudinal coordinate (ϕ):

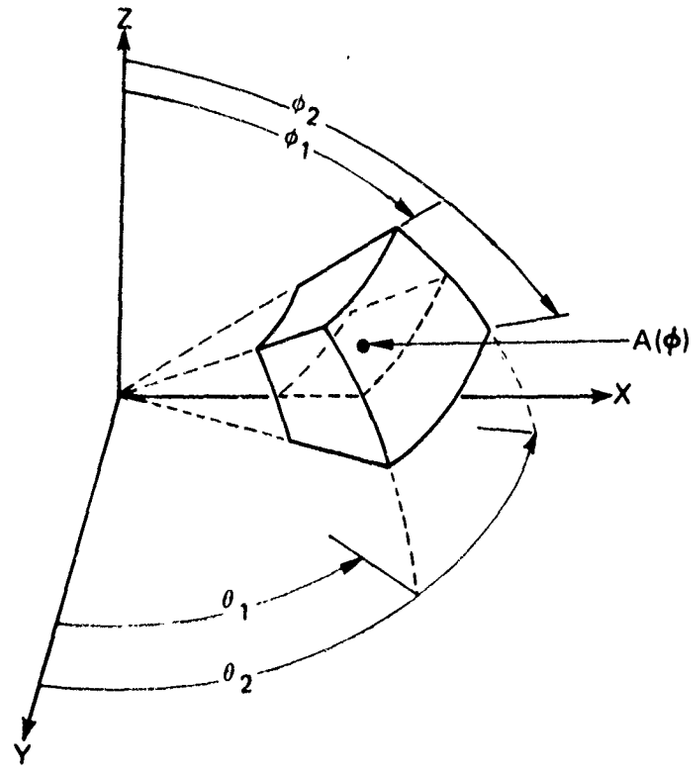

In the following, $T_1 = T(\phi_1)$, $T_2 = T(\phi_2)$, and the node centers are located at (ϕ_1, r, θ) and (ϕ_2, r, θ), where θ is the average

meridional coordinate $((\theta_1 + \theta_2)/2)$. The area normal to the ϕ direction is given by

$$A(\phi) = \frac{\sin \phi \, (r_o^2 - r_i^2) \, (\theta_2 - \theta_1)}{2} \quad ,$$

where r_o is the radius of the outer surface of the nodes and r_i is the radius at the inner surface of the nodes; hence $r_o - r_i$ is the radial thickness of the nodes. Using only the ϕ direction terms for the spherical gradient operator (c.f. Eq. (7)),

$$\dot{q}(\phi) = -A(\phi) \, k \, (1/r) \, dT/d\phi .$$

The previous relationship for $T(\phi)$ combined with the boundary conditions will give

$$\frac{dT}{d\phi} = \frac{\sin \phi \, (T_2 - T_1)}{(\cos \phi_2 - \cos \phi_1)} \quad .$$

Combining the $A(\phi)$ and $dT/d\phi$ relationships will yield

$$\dot{q}(\phi) = \frac{-(r_o - r_i) \, (\theta_2 - \theta_1) \, k \, (T_2 - T_1)}{\ln \left[\frac{\tan (\phi_2/2)}{\tan (\phi_1/2)} \right]} \quad ,$$

giving an effective A/L in the ϕ direction of

$$\left. \frac{A}{L} \right|_{\phi} = \frac{(r_o - r_i) \, (\theta_2 - \theta_1)}{\ln \left[\frac{\tan (\phi_2/2)}{\tan (\phi_1/2)} \right]} \quad .$$

When considering only heat conducted in the radial direction, the divergence of the temperature field (T) for spherical geometries can be reduced to

$$d^2T/dr^2 + (2/r)\ dT/dr = 0 \ .$$

To find T(r), let $p = dT/dr$, so that

$$dp/dr + 2p/r = 0 \ .$$

Further, if $p = C/r^2$, then by substitution in the previous equation

$$-2Cr^3 + (2/r)\ (C/r^2) = 0 \ ,$$

which is an identity, verifying the choice $p = C/r^2 = dT/dr$. One integration of this relationship gives

$$T(r) = (-C/r) + D \ ,$$

where C and D are constants determined by the boundary conditions imposed as illustrated in the following sketch:

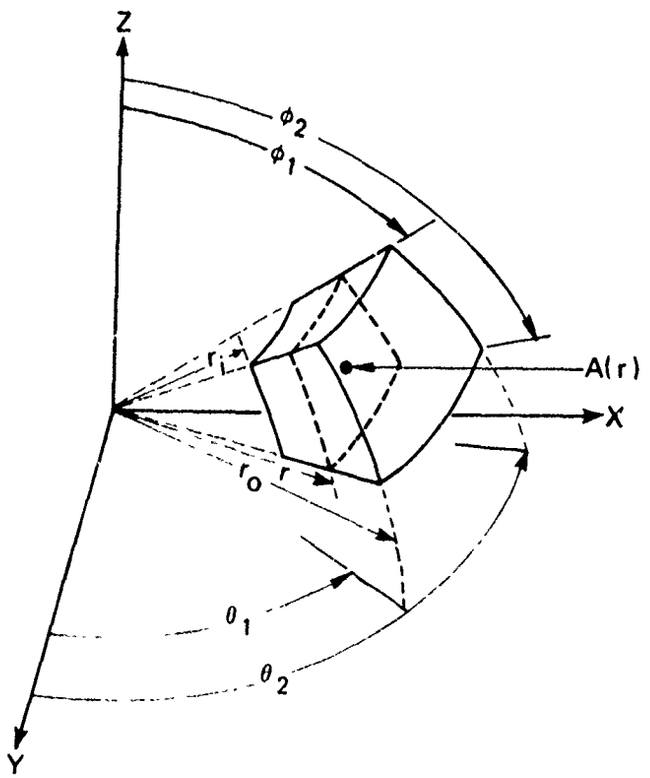

In the sketch, two spherical nodes are in contact at radius r and have node centers at r_o and r_i. The temperature (which depends only on the dimension r) is T_o at r_o and T_i at r_i. Substituting these values as boundary conditions gives

$$C = \frac{T_2 - T_1}{\frac{1}{r_1} - \frac{1}{r_2}} \quad ,$$

and

$$\frac{dT}{dr} = \frac{T_2 - T_1}{r^2\left(\frac{1}{r_1} - \frac{1}{r_2}\right)} \quad .$$

The area normal to the radius direction is given by:

$$A(r) = r^2 \, (\cos \phi_1 - \cos \phi_2) \, (\theta_2 - \theta_1) \quad .$$

The heat conducted across the area at radius r is then

$$\dot{q}(r) = -A(r) \, dT/dr$$

$$= \frac{(\cos \phi_1 - \cos \phi_2) \, (\theta_2 - \theta_1) \, k \, (T_2 - T_1)}{\frac{1}{r_1} - \frac{1}{r_2}} \quad .$$

By inspection with the rectangular case, the effective A/L for this condition is:

$$\left.\frac{A}{L}\right|_r = \frac{(\cos \phi_1 - \cos \phi_2) \, (\theta_2 - \theta_1)}{\frac{1}{r_1} - \frac{1}{r_2}}$$

When the only dependence of temperature is in the longitudinal direction (θ) then the divergence operator on T yields

$$\csc^2 \phi \frac{\partial^2 T}{\partial \theta^2} = 0 ,$$

which reduces to

$$d^2T/d\theta^2 = 0 ,$$

and is identical to the rectangular case. Moreover, it is apparent that the area perpendicular to the θ coordinate does not vary with θ as can be seen in the attendant sketch:

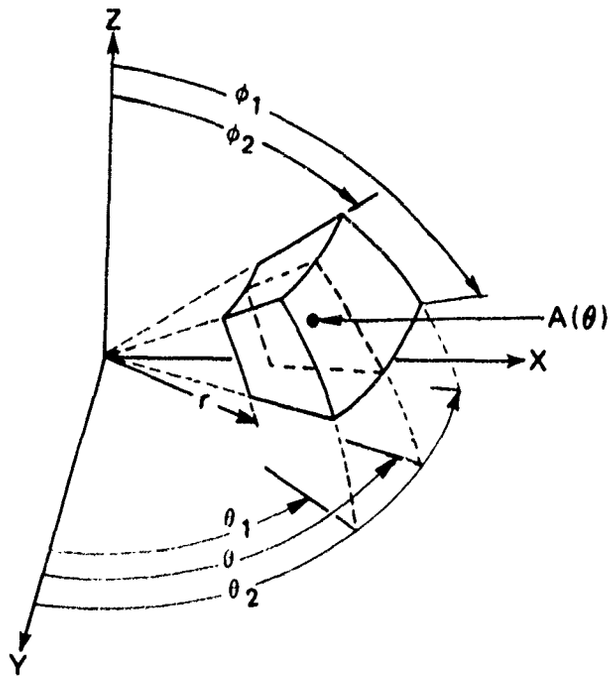

From the simple form of the divergence of T (stated above), by inspection

$$dT/d\theta = \frac{T_2 - T_1}{\theta_2 - \theta_1}$$

with T_1 being the nodal temperature at θ_1, and T_2 being the nodal temperature at θ_2. The contact area between the nodes is at θ; the area perpendicular to the θ coordinate is:

$$A(\theta) = \frac{(\phi_2 - \phi_1)\,(r_o^2 - r_i^2)}{2} \quad ,$$

and the heat conducted through this area is then

$$\dot{q}(\theta) = -A(\theta)\,\frac{k}{r \sin\phi}\,\frac{dT}{d\theta}$$

$$= \left[\frac{(\phi_2 - \phi_1)\,(r_o - r_i)}{\sin\left(\frac{\phi_1 + \phi_2}{2}\right)(\theta_2 - \theta_1)}\right] k\,(T_2 - T_1) \quad .$$

The term in brackets is seen as the actual A/L for the meridional direction if $r = (r_o + r_i)/2$, $\phi = (\phi_1 + \phi_2)/2$, A is given by $A(\theta)$ above, and L is the arc length $(r \sin\phi)\,(\theta_2 - \theta_1)$.

In summary, by taking proper consideration for curvature in cylindrical and spherical coordinate systems, effective A/L formulas have been derived that should be used in the finite difference equations for heat conduction. The terms derived reduce to the correct partial differential equations in the limit of infinitely small differences.

STEADY-STATE TEMPERATURE FIELDS

Iterative Solution

In the steady state there is no change of temperature from one time to the next so that $T = T'$ in Eq. (56) and we have no net flow of heat at any given node; i.e.,

$$\overline{Q} = 0 \quad , \tag{62}$$

which states that the net heat flow for each node must be zero. Solving the steady-state problem then involves finding the set of

temperatures ($\bar{T}$) so that Eq. (62) is satisfied. Since all of the individual terms that comprise Eq. (62) are temperature dependent (c.f. Eqs. (57) through (59)), then $\bar{Q}$ is a function of $\bar{T}$; i.e.,

$$\bar{Q} = F(\bar{T}) \ . \tag{63}$$

Newton's method for finding the zeros of a function can be used to solve this system of equations in the following way: If an initial guess for $\bar{T}$, say $\bar{T}_0$, is substituted in Eq. (63), then

$$\bar{Q}_0 = F(\bar{T}_0) \neq 0 \ . \tag{64}$$

A set of correction terms ($\bar{\delta}_0$) will exist so that $\bar{T}_0 - \bar{\delta}_0 = \bar{T}$ and

$$F(\bar{T}) = 0 \ ,$$

or

$$F(\bar{T}_0 - \bar{\delta}_0) = 0 \ . \tag{65}$$

Equation (65) is expanded in a Taylor's series as

$$F(\bar{T}_0 - \bar{\delta}_0) = F(\bar{T}_0) - \bar{\delta}_0 F'(\bar{T}_0) + \frac{\bar{\delta}_0^{\,2} F''(\bar{T}_0)}{2!} - \ldots = 0 \ , \tag{66}$$

where the primes indicate derivatives with respect to temperature.

It is assumed that the initial guess ($\bar{T}_0$) is sufficiently accurate so that the corrections ($\bar{\delta}_0$) are small. Further, the second and all higher derivative terms are assumed small compared with the first derivative term. With this assumption Eq. (66) is solved for $\bar{\delta}_0$:

$$\bar{\delta}_0 \approx \frac{F(\bar{T}_0)}{F'(\bar{T}_0)} \ . \tag{67}$$

Because of the approximations, Eq. (67) can be written as

$$\bar{\delta}_1 = \frac{F(\bar{T}_0)}{F'(\bar{T}_0)} \quad , \tag{68}$$

and moreover,

$$\bar{T}_0 - \bar{\delta}_1 = \bar{T}_1 \quad , \tag{69}$$

where $\bar{\delta}_1$ is an approximation to the true correction terms $(\bar{\delta}_0)$, and T_1 is an approximation to the true steady-state temperatures T. Combining Eqs. (68) and (69) yields:

$$\begin{aligned} \bar{T}_1 &= \bar{T}_0 - [F(\bar{T}_0)/F'(\bar{T}_0)] \\ &= \bar{T}_0 - \bar{Q}_0/\bar{Q}'_0 \quad . \end{aligned} \tag{70}$$

An iterative process can be devised wherein each set of temperatures $\bar{T}_1$ are substituted back into Eq. (62), new values for $F(T_1)$ and $F'(T_1)$ are used in Eq. (70) to find a further improved set of temperatures $(\bar{T}_2)$. The process is repeated in this manner until the corrections $(\bar{\delta}_1)$ approach zero and the steady-state heat flows $(\bar{Q})$ equal zero. Error tolerances for the δ_1 values on the order of $\pm 1°R$ have been used successfully in practice; the precise value is selectable when the program is executed.

To accomplish the steady-state solution in this manner, it is required to have an initial guess $(\bar{T}_0)$ and to evaluate the N correction factors (Q_0/Q'_0). The heating rate for each node $(\bar{Q})$ is calculated as discussed above for the transient solution and the derivatives $(\bar{Q}')$ are calculated as follows:

Conduction

$$\frac{\partial \dot{q}_c}{\partial T_n} = \frac{\partial}{\partial T_n}\left[\sum_{i=1}^{K} \frac{kA}{L}\bigg|_{n-i} (T_n - T_i)\right]$$

$$= \sum_{i=1}^{K} \frac{kA}{L}\bigg|_{n-i} + \sum_{i=1}^{K} (T_N - T_i)\, \frac{A}{L}\bigg|_{n-i} \frac{\partial k_{n-i}}{\partial T_n} \quad . \qquad (71)$$

Radiation

$$\frac{\partial q_R}{\partial T_n} = \sigma \frac{\partial}{\partial T_n}\left[\sum_{i=1}^{R} F_{n-i}\, A_{n-i}\, \epsilon_{n-i} \left(T_n^4 - T_i^4\right)\right]$$

$$= \sigma \left[\sum_{i=1}^{R} F_{n-i}\, A_{n-i}\, \epsilon_{n-i}\, 4T_n^3 + \sum_{i=1}^{R} F_{n-i}\, A_{n-i} \left(T_n^4 - T_i^4\right) \frac{\partial \epsilon_{n-i}}{\partial T_n}\right] . \qquad (72)$$

External Fluxes and Internal Heat Generation

$$\frac{\partial \sum_{i=1}^{Q''} q''_{n-i}}{\partial T_n} = 0 \quad \text{and} \quad \frac{\partial q'''}{\partial T_n} = 0 \quad , \qquad (73)$$

by definition.

Composite Conduction

$$\frac{\partial q_{cc}}{\partial T_n} = \frac{\partial \sum_{i=1}^{C} K_{cc} (T_n - T_i)}{\partial T_n} = \sum_{i=1}^{C} (T_n - T_i) \frac{\partial K_{cc}}{\partial T_n} + \sum_{i=1}^{C} K_{cc} \quad . \quad (74)$$

It can be seen from Eq. (57) that

$$\frac{\partial k_{n-i}}{\partial T_n} = \frac{f'_1 (T_n + T_i)/2}{2} \quad , \quad (75)$$

and similarly, from Eq. (58),

$$\frac{\partial \varepsilon_{n-i}}{\partial T_n} = \frac{f'_2 (T_n + T_i)/2}{2} \quad . \quad (76)$$

With Eqs. (59a), (75), and (76) substituted into Eqs. (71) through (74), the iterative process implied by Eq. (70) may be carried out to arrive at the steady-state temperature distribution.

Usage experience with this iterative solution technique has been varied. In general the following cautions are offered (1) The number of iterations required for solution depends strongly on the initial guess for the temperature field (T_0); (2) the larger the number of nodes, the more iterations will be required and the smaller the probability of satisfactory convergence; and (3) a constant relaxation factor (described below) may improve convergence speed and solution accuracy.

Relaxation Factor

A provision has been added that allows Eq. (70) to be written as

$$\bar{T}_1 = \bar{T}_0 - R(\bar{Q}_0 - Q_0) \quad , \quad (77)$$

where R is a constant relaxation factor. Simply stated, values of R greater than 1 tend to accelerate the convergence to solutions that otherwise require many iterations and values of R less than 1 tend to damp successive solutions to problems that tend to oscillate. Oscillation can be characterized by successive values of δ being positive and then negative, and not diminishing in absolute value. The proper choice for R is a subject of extensive mathematical significance and is generally found by experience (i.e., trial and error).

The foregoing comments serve to indicate an inherent undesirability in the iterative technique just described — its unpredictable behavior. To avoid this, another scheme is available — the implicit technique — and is described next.

Implicit Technique

The right side of Eq. (55) describes heat transferred via internal conduction, but there also may be radiation transfer, as well as independently specified external heat fluxes or internal heat generation. Terms such as these enter Eq. (55) either as constants or terms that may have some dependence on T_n. The specific form of these terms is described above for the transient solutions. It will be sufficient for purposes of description to examine the internal conduction term as written in Eq. (55) and note that the other terms mentioned simply add to the coefficients in the equations that will be developed.

Note that in the steady state, T'_n equals T_n (there is no change in temperature with time) and the left side of Eq. (55) is zero. Equation (55) is expanded to

$$\sum_{i=1}^{K} \frac{k_{n-i} A_{n-i}}{L_{n-i}} T_n - \sum_{i=1}^{K} \frac{k_{n-i} A_{n-i}}{L_{n-i}} T_i = 0 . \qquad (78)$$

For every node in the network an equation of the form of Eq. (78) can be written. For boundary nodes whose temperatures (T_b) are known, Eq. (78) is not relevant and the following form is used:

$$T_b = \text{constant} . \qquad (79)$$

For a constant flux or internal heat generation boundary condition, the heat flux is simply added to the left side of Eq. (78) as a constant. It should be noted that in the case of convective heat fluxes a separate subroutine (SAERO) uses an implicit technique to solve for the surface temperature. Therefore, as far as the nodal network solutions are concerned, convective surface temperatures enter as equations such as Eq. (79). It is now clear that for a network of N node points, N equations of the form of Eq. (78) can be written. To find all N unknown temperatures requires the simultaneous solution of this system of equations. Written in matrix form the system of equations is

$$
\begin{array}{c}
\text{Eq. No.} \\
1 \\ 2 \\ 3 \\ \cdot \\ \cdot \\ \cdot \\ \cdot \\ n \\ \cdot \\ b \\ \cdot \\ \cdot \\ N
\end{array}
\begin{bmatrix}
C_{11} & C_{12} & C_{13} & \cdots & C_{1n} & \cdots & C_{1N} \\
C_{21} & C_{22} & C_{23} & \cdots & C_{2n} & \cdots & C_{2N} \\
C_{31} & C_{32} & C_{33} & \cdots & C_{3n} & \cdots & C_{3N} \\
\cdot & \cdot & \cdot & & \cdot & & \cdot \\
\cdot & \cdot & \cdot & & \cdot & & \cdot \\
\cdot & \cdot & \cdot & & \cdot & & \cdot \\
\cdot & \cdot & \cdot & & \cdot & & \cdot \\
C_{n1} & \cdot & \cdot & \cdots & C_{nn} & \cdots & C_{nN} \\
\cdot & \cdot & \cdot & & \cdot & & \cdot \\
0 & 0 & 0 & \cdots & 0 & \cdots & 0 \\
\cdot & \cdot & \cdot & & \cdot & & \cdot \\
\cdot & \cdot & \cdot & & \cdot & & \cdot \\
C_{N1} & C_{N2} & C_{N3} & \cdots & C_{Nn} & \cdots & C_{NN}
\end{bmatrix}
\times
\begin{bmatrix} T_1 \\ T_2 \\ T_3 \\ \cdot \\ \cdot \\ \cdot \\ \cdot \\ T_n \\ \cdot \\ T_b \\ \cdot \\ \cdot \\ T_N \end{bmatrix}
=
\begin{bmatrix} 0 \\ 0 \\ 0 \\ \cdot \\ \cdot \\ \cdot \\ \cdot \\ 0 \\ \cdot \\ \text{Constant} \\ \cdot \\ \cdot \\ -Q_{ext} \end{bmatrix}
$$

The above system shows nodes 1 through N as regular internal nodes, a boundary node with value T_b, and node N with an externally supplied heat flux (Q_{ext}).

It should be noted that the off-diagonal coefficients are symmetric; i.e.,

$$C_{i,j} = C_{j,i} = \frac{k_{i,j} A_{i,j}}{L_{i,j}} = H_{i,j} \quad ,$$

and that the diagonal coefficients are

$$C_{nn} = - \sum_{i=1}^{K} \frac{k_{n-i} A_{n-i}}{L_{n-i}} .$$

The solution technique used to solve these simultaneous equations is Gaussian elimination with back substitution. In this technique the equations are algebraically manipulated so that the coefficient matrix is reduced to upper triangular (i.e., 1's occurring along the diagonal with all zeros below the diagonal). This is accomplished, for example, by: (1) dividing the first equation by $C_{1;}$; (2) multiplying the new equation 1 by $-C_{21}$ and adding the result to equation 2, thus producing a zero for C_{21}; (3) dividing the new equation 2 through by the new C_{22}. Proceeding in this manner through all N equations produces the upper triangular coefficient matrix. Note that at the end of this procedure, the last equation (N) will read

$$\begin{array}{c} \text{Eq. No.} \\ \cdot \\ \cdot \\ N-1 \\ N \end{array} \quad \begin{bmatrix} \cdot & \cdot & \cdot & \cdot \\ \cdot & 1 & \cdot & \cdot \\ \cdot & 0 & 1 & C_{N-1,N} \\ \cdot & 0 & 0 & 1 \end{bmatrix} \times \begin{bmatrix} \cdot \\ \cdot \\ T_{N-1} \\ T_N \end{bmatrix} = \begin{bmatrix} \cdot \\ \cdot \\ \cdot \\ \text{value} \end{bmatrix}$$

which says T_N = value. This result can then be substituted into equation number N-1, and T_{N-1} can be solved for. This back substitution procedure can be followed up through the reduced equations until all N temperatures are known.

While this technique requires the storage of the N × N coefficient matrix, usage has shown that solutions are achieved much quicker and are generally more accurate than the iterative scheme described earlier.

It should be mentioned that the implicit technique is also used iteratively; i.e., successive solutions to the temperature field are compared and convergence is judged according to the successive differences. Since the values in the coefficient matrices are temperature dependent, successive coefficient matrices will not in general be identical until the temperatures themselves do not

change. Generally, the number of iterations required is small (less than 10).

INTERPOLATION TECHNIQUES

In arriving at the transient or steady-state temperature response of a thermal network the routines in URLIM make extensive use of numerical interpolation. Because all of the pertinent material properties are allowed to have temperature (and sometimes pressure) dependence, these functional relationships must be modeled. The technique employed here is the most simple and direct; the functions are represented by tables of independent and dependent variable values and linear interpolation is most frequently used. The table look-up procedure most often employed is a simple serial search. In general, the tables can be as long as required to accurately define the particular function. Search time will increase with increases in tabular length. The following discussion will outline the techniques used by the URLIM interpolators. The PIF1, PIF1D, and DECIDE routines in particular use the following scheme.

Let the independent variable be represented by the vector of N values $\bar{X}$ and the dependent variable by the vector of N values $\bar{Y}$ with the functional relationship between the values expressed as.

$$\bar{Y} = f(\bar{X}) \quad .$$

Each value in $\bar{Y}$, Y_i has a corresponding value in $\bar{X}$, X_i so that

$$Y_i = f(X_i) \quad ,$$

and each pair X_i, Y_i is a point on the curve

$$y = f(x) \quad .$$

If a value of x is given (x_0) and the corresponding value of y (y_0) is required, then a search is performed through the values $\bar{X}$ until two values are found:

$$X_i \leq x_0 < X_{i+1} \quad .$$

Note that the vector $\bar{X}$ must contain values in monotonic increasing order. When the two points that satisfy the inequality above are found the value y_0 is computed as

$$y_0 = Y_i + \left(\frac{Y_{i+1} - Y_i}{X_{i+1} - X_i}\right)(x_0 - X_i) \quad .$$

In the cases where $x_0 < X_1$ or $x_0 > X_N$ (where X_N is the last tabular value in the vector $\bar{X}$) linear extrapolation is employed using the two given end point values.

The routine LINLOG uses a modified version of the same method described above. In this case, after the two tabular values X_i and X_{i+1} are found the corresponding values Y_i and Y_{i+1} are replaced in the calculations by ln (Y_i) and ln (Y_{i+1}), respectively. The returned value y_0 is then

$$y_0 = \exp\left[\ln Y_i + \left(\frac{\ln Y_{i+1} - \ln Y_i}{X_{i+1} - X_i}\right)(x_0 - X_i)\right] \quad .$$

This result is then a semilogarithmic linear interpolation. For values of y that are negative, the sign is retained and the ln function is performed on the absolute values of X. In the special case of the value of either Y_i or Y_{i+1} lying between +1 and -1, the logarithmic functions are suspended and simple linear interpolation is performed.

In the BIVLID routine, the functional dependence of a variable on two independent variables is modeled. In this case the two independent variables x_1 and x_2 have monotonically increasing values stored in the vectors $\bar{X}_a$ and $\bar{X}_b$ with individual values $X_{a_i} = X_a$ and $X_{b_j} = X_b$. The dependent variable y is defined as $y = f(x_a, x_b)$ and is represented in the two-dimensional array $\bar{\bar{Y}}$. The subscripts i and j are used to index the array $\bar{\bar{Y}}$ (e.g., $Y_{i,j} = f(X_a, X_b)$). The subscript i is used to index the vector $\bar{X}_a$ and the first index position of the array $\bar{\bar{Y}}$; similarly, the subscript j is used to index the vector $\bar{X}_b$ and the second index position of $\bar{\bar{Y}}$.

When values of x_a and x_b are given, BIVLID scans the vectors $\bar{X}_a$ and $\bar{X}_b$, respectively, until the following conditions are satisfied:

$$(1) \quad X_{a_i} \leq x_a < X_{a_{i+1}} ,$$

$$(2) \quad X_{b_j} \leq x_b < X_{b_{j+1}} .$$

The above conditions define i and j uniquely. In the case where $x_a < X_{a_1}$, i is set to 1. Also when $x_a > X_{a_n}$, where n is the extent of the vector $\bar{X}_a$, then i is set to n. Exactly analogous conditions hold for the vector $\bar{X}_b$ and j.

With the values i and j established, two intermediate values of the dependent variable are found:

$$Y'_1 = Y_{i,j} + \left(\frac{Y_{i,j+1} - Y_{i,j}}{X_{b_{j+1}} - X_{b_j}} \right) \left(x_2 - X_{b_j} \right) ,$$

$$Y'_2 = Y_{i+1,j} + \left(\frac{Y_{i+1,j+1} - Y_{i+1,j}}{X_{b_{j+1}} - X_{b_j}} \right) \left(x_2 - X_{b_j} \right) .$$

The required value of y is then computed as

$$y(x_1,x_2) = Y'_1 + \left(\frac{Y'_2 - Y'_1}{X_{a_{i+1}} - X_{a_i}} \right) \left(x_1 - X_{a_i} \right) .$$

The BIVLID routine also returns either of the partial derivatives of the function y depending on the value of a control code. In the example shown above the derivative would be

$$\frac{\partial y}{\partial x_1} = \frac{Y'_2 - Y'_1}{X_{a_{i+1}} - X_{a_i}} \quad .$$

Similar expressions to the ones above can be written for cases where $\partial y/\partial x_2$ are required.

The routine has a facility for returning a value for one of the independent variables when values for the dependent variable and the other independent variable are supplied. This function is termed an "inverse" interpolation and is useful in certain applications. In this process if the value x_a is given along with the value $y(x_a, x'_b)$, then the value x'_b is returned. The vector $\bar{X}_a$ is searched until

$$X_{a_i} \leq x_a < X_{a_{i+1}} \quad ,$$

thereby establishing the value of i and two vectors of dependent values, namely $Y_{i,*}$ and $Y_{i+1,*}$. A series of intermediate dependent variable values are then found between these two vectors; i.e.,

$$Y'_1 = Y_{i,j} + \left(\frac{Y_{i+1,j} - Y_{i,j}}{X_{a_{i+1}} - X_{a_i}}\right)\left(x_1 - X_{a_i}\right) \quad ,$$

and

$$Y'_2 = Y_{i,j+1} + \left(\frac{Y_{i+1,j+1} - Y_{i,j+1}}{X_{a_{i+1}} - X_{a_i}}\right)\left(x_1 - X_{a_i}\right) \quad ,$$

such that either

$$(1) \quad Y'_1 \leq y(x_1, x'_2) < Y'_2 \quad ,$$

or

$$(2) \quad Y'_1 \geq y(x_1, x'_2) > Y'_2 \quad .$$

When either of these conditions is true, then a value for the index j will be implicitly known. The returned value of the dependent variable (x'_2) is then given as:

$$x'_2 = X_{b_j} + \left(\frac{y(x_1, x'_2) - Y'_1}{Y'_2 - Y'_1} \right) \left(X_{b_{j+1}} - X_{b_j} \right) .$$

A similar procedure can be outlined when the values $y(x'_1, x_2)$ and x_2 are given and x'_1 is desired.

If the conditions (1) and (2) are not satisfied after all values of j are used, then the dependent variable value that was given lies beyond the tabulated values. In such cases, the routine will generate an appropriate warning message and return the last tabulated value of the required independent variable (i.e., X_{a_m} or X_{b_n}, where m (or n) is the extent of the vector X_a (or X_b)).

In cases where the dependent variable is double valued (i.e., there is more than a single value of j that satisfies the conditions of (1) or (2) above), then the smallest such value of j will be used.

When the data being used for interpolation have an inherent logarithmic dependence, a linear-logarithmic interpolation may be obtained in much the same way as done for the single independent variable data in LINLOG, discussed earlier. For these cases the BIVLLID routine is used, which has the same basic algorithm as discussed above for BIVLID. The logarithmic aspect is accomplished by using the logarithm of the dependent variable values rather than the values themselves. In other words, where $Y_{i,j}$ is used in the relations above, $\ln(Y_{i,j})$ is substituted and the returned values are the antilogs of the resultant values.

INTEGRATION

Within the thermal-stress routines (SIGMA and SIGMET) numerical integrations are required of various tabular functions. The process is accomplished by the TRAP routine and essentially evaluates the integral I, which is defined as

$$I = \int_a^b F(x)\, dx \quad .$$

The function F(x) is assumed represented in tabular form (i.e., a vector of independent variable values ($\bar{X}$) and a corresponding vector of dependent variable values ($\bar{Y} = F(\bar{X})$).

The algorithm divides the interval [a,b] in half and the three functional values $y_1 = f(a)$, $y_2 = f[(a+b)/2]$, and $y_3 = f(b)$ are found by interpolation. The integral I is now approximated by the area under the three-point function via the trapezoidal rule; i.e.,

$$I_2 = (y_1 + y_2)\,(b - a)/4 + (y_2 + y_3)\,(b - a)/4 \quad .$$

The interval [a,b] is now divided into three parts and the values

$$y_1 = f(a),$$

$$y'_2 = f(2a + b)/3,$$

$$y'_3 = f(2b + a)/3, \text{ and}$$

$$y_4 = f(b)$$

are determined by interpolation. The integral is approximated again by the trapezoidal process and is called I_3. At this point the value $E = 1 - |I_2/I_3|$ is compared with a preset tolerance value of 0.01. If $E > 0.01$ then the interval is divided into fourths, the approximation I_4 is generated via the trapezoidal rule, and a new value of $E = 1 - |I_3/I_4|$ is compared. This process is continued until either $E \leq 0.01$ or 20 such iterations have occurred. If, after 20 iterations, E is greater than 0.01 then an appropriate message is printed, the ratio I_{20}/I_{19} is printed, and the value I_{20} is used as the value of the integral.

SIMULTANEOUS AND IMPLICIT EQUATIONS

Within the aerodynamic heating routines, there is a requirement for the solution to implicit equations (i.e., equations with

terms or functions of the unknown variable on both sides of the equal sign that cannot be solved in closed form). Also, in the iterative steady-state solution procedure, a number of implicit equations must be solved simultaneously. The numerical technique used in both cases is Newton's method wherein successive corrections are calculated for the value of the unknown quantity based on partial derivatives. A complete description of this algorithm is presented in the paragraph entitled "Steady-State Temperature Fields" (Section 2).

The set of simultaneous equations generated in the implicit steady-state method are solved by Gaussian elimination to achieve an upper triangular coefficient matrix and the unknowns (temperature) are solved for by back-substitution. Again, this method is described in Section 2 and will not be repeated here.

3. DATA MANAGEMENT

EXTERNAL STORAGE

In the URLIM and SHTP subroutine library it has been found useful to have a number of variables that can be accessed freely among the subroutines. This class of variables is called EXTERNAL in the PL/I language. Table 2 of Volume 2 of this report lists all of the EXTERNAL variables used with brief descriptions. Since EXTERNAL variables must have unique names, the list will serve as a guide to future changes in the program that may require additional EXTERNAL variables.

DYNAMIC STORAGE

Many of the arrays of data stored by the URLIM routines are of flexible extent; i.e., their dimensions are program variables and are changed as required from run to run. Many examples are evident in Table 2 (e.g., the nodal temperatures (T) and the steady-state coefficient matrix (HMAT). As might be expected, the single most important value that determines the extent of the various arrays is the number of thermal nodes (i.e., the value of variable LASCAP). Subroutine STORE is the routine that allocates the bulk of the required dynamic storage according to the parameters passed to it. In establishing the storage limits that will be required, one of the important aspects to manage is the use by the READCP routine of "node" numbers that are beyond the value LASCAP. In describing the network data it is possible to use an extended input technique that will require additional storage (c.f. Appendix F of Vol. 1 of this report). When employing this method, adequate storage must be allocated by the STORE routine through the parameter XCAPLIM. Further explanations can be derived from the discussion of the STORE routine (Appendix H of Vol. 1 of this report).

The use by the SIGMA, SIGMET, and MOBSER routines of nodal temperature positions in the vector T must also be allowed for if the plotting flag is set in the calling sequence to any of these routines. This feature does not require storage additional to that set by LASCAP, but it is imperative that the "node" number used for the thermal stress values not be the number of a node in the network.

Another important data management technique employed within URLIM is the use of POINTER variables to locate the storage of the various material property tables and the various time-dependent tables. In the case of the thermal properties, the READKK routine

stores the memory locations of the property data it reads into the EXTERNAL POINTER variable PP. The values in PP are then made available to the routines that require the thermal property tables. Indexing with the vector PP is accomplished via the ID values supplied to the READRK routine (i.e., the material thermal property codes).

For the time-dependent variables read in by the READTM routine, the EXTERNAL POINTER array TMPNTR is used to store the locations of the tabular data. This storage information is then made available to routines in the URLIM library for processing. The indexing of TMPNTR, a two-dimentional array, is first by the ID number used when read by READTM and then by the dependent variable position in the calling sequence. To illustrate, consider the following hypothetical call to routine READTM:

```
CALL READTM (ID#, TM, DEP1, DEP2, DEP3, DEP4, DEP5,
             #ENT, INFILE):
```

where the vector TM is the list of time values and the vectors DEP1 through DEP5 are corresponding lists of dependent variable values. Upon return from this call to READTM the storage locations of the variable TM and DEP1 through DEP4 will be recorded in the values of TMPNTR (ID#, 1 through 5), respectively.

The Initial Storage Area

One of the "optimizing" features of the PL/I optimizing compiler is its improved ability to manage the dynamic allocation of storage, according to the requirements of the particular program. The computer code that supervises the allocation of storage segments for a particular program is supplied automatically by the optimizer compiler; the only item supplied by the user is the specification of the amount of storage that will be needed for the dynamic storage. This area is termed the initial storage area (ISA) and has a default value in the present compiler implementation of 8000 bytes. For most programs, and certainly for the URLIM program, this is an insufficient size for the ISA. Determining the proper ISA size is done with the aid of the program-generated storage report that gives an accounting of the actual storage requirements and the number of times storage outside of the ISA was required. Figure 8 is a reproduction of a typical storage report, the salient features of which are discussed in the following paragraph.

In Fig. 8 the size specified for the ISA is given in bytes; the amount of actual PL/I storage needed by the job is given and

```
STORAGE MANAGEMENT REPORT

          ISASIZE SPECIFIED 13312 BYTES

          LENGTH OF INITIAL STORAGE AREA (ISA) 13312 BYTES

          AMOUNT OF PL/I STORAGE REQUIRED 11544 BYTES

          AMOUNT OF STORAGE OBTAINED OUTSIDE ISA 0 BYTES

          NUMBER OF GETMAINS 0

          NUMBER OF FREEMAINS 0

          NUMBER OF GET NON-LIFO REQUESTS 46

          NUMBER OF FREE NON-LIFO REQUESTS 4

END OF REPORT
```

Fig. 8 Storage Report from PL/I Optimizing Compiler

the amount of storage used outside o. the ISA is given. Further, in cases where storage outside the ISA is required, the number of requests to the system (OS) for such storage is indicated. In a program with a properly specified ISASIZE, the amount of storage required outside the ISA will be zero (i.e., the amount of PL/I storage required and the ISA will be equal). To establish the correct value of the ISA, an estimate of the proper size is made and a report is asked for via the PARM field of the EXEC card for the job. Upon receipt of the report, the correct amount of PL/I storage required will be known, and subsequent runs should use this value as the ISASIZE. If program variables that affect the dynamic storage are changed between runs, the amount of proper ISA storage may change. For this reason, it is generally good practice to have storage reports made with each run and make adjustments to the ISASIZE as required.

INTERFACE WITH THE OPERATING SYSTEM

The machine configuration for the URLIM program code and the SHTP subroutines is the IBM 360. The PL/I source was compiled with the optimizer version of the PL/I compiler. All of the routines used by URLIM or contained in the SHTP library are available as load modules. Also, the URLIM main program is available as a load module. The extent of interaction with the IBM operating system (OS) is then to properly assemble the required subroutine modules and execute the program. The discussions that follow will be applicable to the running of URLIM or to the execution of another application program using the SHTP library, with the following difference. For URLIM runs, the main program is already written, compiled, and stored in a data set; for a run with SHTP modules, the main program will be user-supplied and assumed available as a precompiled load module ready for use.

To further preface the following discussions, a general description of the IBM 360 system environment will be made. OS is fundamentally a supervisory program that oversees the allocation of the 360's basic resources, namely central processor unit (CPU) time, main storage (region), and peripheral storage devices. Interaction with OS is accomplished by writing statements in job control language (JCL). These statements serve as preparatory remarks to OS in that they identify the job to be run and make requests for some of the three aforementioned basic resources. There are three fundamental types of JCL statements: (1) the JOB card (containing user identification and accounting information) that serves to identify distinct jobs to OS; (2) EXEC cards that identify what program is to be run, and (3) data definition (DD)

cards that identify the various files (data-sets) that will be required by the program. Requests for region (addressable storage) and CPU time are made on the EXEC card.

At any given 360 installation there will be a set of programs that are used very frequently by many users. The attendant JCL (which may be quite lengthy) is often contained in files known as "cataloged procedures." These high-usage programs generally include the IBM-supplied high-level compilers (PL/I, Fortran, etc.), the link-editor program, and others. The JCL described here will include (1) that which is needed to use the link-editor and (2) that which is sufficient to run a previously link-edited module.

The Link-Editor

The cataloged procedure OL used at the IBM 360/91 installation at APL is used to execute the link-editor; OLG is used to execute the link-editor and then execute the resultant program. The use of procedure OL is shown in the example below. OL is used to assemble the required load modules together and save the resultant, fully link-edited program on the file described by the L.SYSLMOD DD card:

```
//   EXEC OL,'LIB=BBE.FRAZER.BASICO2',
//        PARM.L='LIST,MAP,LET'
//L.SYSLMOD DD DSN=xxx.xxx.xxx(yyy),
//          DISP=(NEW,CATLG),
//          SPACE=(3156,(60,20,2),RLSE),
//          UNIT=SAVE
//L.SYSIN   DD *
     INCLUDE SYSLIB (URLIM)
     ENTRY PLISTART
/*
```

The example first names the cataloged data set BBE.FRAZER.BASICO2 as the SYSLIB file for the link-editor. Next, the file SYSLMOD is designated to be data set xxx.xxx.xxx(yyy) (i.e., member yyy of the partitioned data set xxx.xxx.xxx). Further, the data set xxx.xxx.xxx is to be saved via cataloging for later use. The "PARM.L=" specifies operating conditions for the link-editor, namely, that a storage map is requested (MAP) and will be printed by the link-editor; that all input to the link-editor will be listed (LIST); that the link-editor shall continue its operation even though an error may occur (LET).

The input file to the link-editor program (//L.SYSIN) contains two instructions to the link-editor: (1) to include the member URLIM from the SYSLIB data set and (2) that the entry point

(first executable statement) of the module is named PLISTART, a name provided automatically by the PL/I optimizer compiler and found with the main program. The member URLIM in this example is the main program and will be looked for by the link editor as a member of the partitioned data set described by the SYSLIB DD card in the cataloged procedure OL. All subroutines called by the URLIM program and all subroutines subsequently called are assumed to be members of either the data set BBE.FRAZER.BASICO2, or of the system libraries named automatically within the cataloged procedure OL. The link-editor's output (the complete executable program) is written on the file SYSLMOD and the job is finished. The SYSLMOD definitions indicate to the system that the file is to be saved and cataloged for later use.

The interested reader will find further descriptions of the link-editor program and descriptions of other ways of assembling a complete executable program in Refs. 16 and 17. These other methods include overlay defining to maximize storage use and excluding routines that are referred to but never actually called.

The procedure OLG is used in the same way as procedure OL except that the completely executable program (stored on the SYSLMOD file) is executed in a subsequent JOB step:

```
//     EXEC   OLG,LIB='BBE.FRAZER.BASICO2',
//            PARM.L='LIST,MAP,LET',
//            PARM.G='ISASIZE(11K),R'
//L.SYSLMOD  DD  DSN=xxx.xxx.xxx(yyy),
//            DISP=(NEW,CATLG),UNIT=SAVE,
//            SPACE=(3156,(60,20,2),RLSE)
//L.SYSIN  DD  *
     INCLUDE   SYSLIB(URLIM)
     ENTRY     PLISTART
/*
//G.SYSIN    DD   *
     (input data, as required)
//G.READFIL  DD  DSN=xyz.abc,DISP=SHR
```

The PARM.G statement passes parameters to the executing program and are described in detail in the preceding discussion. The input files required by the program are included at the end of the

---

Ref. 16. "System 360 Model 91 User's Guide," APL/JHU BCS-1:40, November 1973.

Ref. 17. "IBM OS Linkage Editor and Loader," Eleventh Edition, IBM File No. S360/S370-31, Order No. GC28-6538-10, April 1973.

JCL prefixed with "G." to indicate the second job step (named "G") in the same way as the link-editor step files are prefixed with "L."

Complete Executable Programs

Once a complete executable program has been created (as described above or by the use of other cataloged procedures), an execution may be obtained by providing OS with the proper time and region requirements as well as the required file definitions (via DD cards). The JCL given below is an example of what can be specified:

```
//   EXEC   PGM=URLIM,
//          REGION=rrrK,
//          TIME=tt,
//          PARM='ISASIZE(iiiK),REPORT'
//STEPLIB   DD  DSN=xxx.xxx.xxx,DISP=SHR
//PLIDUMP   DD  SYSOUT=A
//SYSIN     DD   *
     (input data to follow here)
/*
//READFIL     DD   DSN=xyz.abc,DISP=SHR
```

In this example, the EXEC card specifies (via the PGM= statement) the member within the PDS named on the STEPLIB card (in this case the data set named xxx.xxx.xxx) that contains the completely executable program. (This example is consistent with the examples above for OL and OLG in that the names coincide.) The EXEC card asks for rrrK (rrr-thousand) bytes ("characters") of storage and requests tt minutes of CPU time. [The time request can be specified in minutes and seconds as "TIME=(mm,ss)"]. Additionally, a parameter is passed to the executing program as "PARM=...." This parameter specifies that the Initial Storage Area (ISA) is to be iiiK bytes long and that a storage report is to be given. The significance of the ISASIZE, and the interpretation of the REPORT are discussed above in the section on Dynamic Storage. The STEPLIB card names the data set containing the program to be executed (URLIM in this instance). The PLIDUMP file is the print file onto which the REPORT will be written. The SYSIN file includes input required by the program and expected from the file SYSIN. The READFIL file is indicative of how files other than SYSIN can be used for supplying input data to the various READ routines (e.g., READRK). These routines, according to values supplied as arguments, can read the required data from any file named by a DD statement included with the JCL for the execution of the job; the

card "//READFIL DD ..." above describes such a file. Other specific examples of these auxiliary files are given in the READ routine usage descriptions in Vol. 2 of this report.

This demonstrates the way in which an URLIM or SHTP program module can be assembled and executed in an IBM OS 360 system environment. There are other ways of accomplishing the same results and the experienced user will experiment with and exploit such avenues that prove beneficial to his needs.

ACKNOWLEDGMENT

The work reported herein is sponsored by the Naval Sea Systems Command (SEA-03513) under Contract No. N00017-72-C-4401. The author appreciates the patient and consistent support of O. Seidman and L. Pasiuk, which has made this work possible. The work was conducted under the guidance of L. B. Weckesser, Supervisor of the Thermal Analysis Section. The author also acknowledges the help of R. W. Nemman and D. Brockelbank for their suggestions and assistance in the development of the computer program.

REFERENCES

1. R. E. Wilson, Handbook of Supersonic Aerodynamics, Sections 13 and 14, "Viscosity" and "Heat Transfer Effects," NAVORD Report 1488, Naval Ordnance Laboratory, White Oak, MD, August 1966.

2. E. R. G. Eckert, "Survey of Boundary Layer Heat Transfer at High Velocities and High Temperatures," Technical Report 59-624, Wright Air Development Center, Dayton, OH, April 1960.

3. A. P. Colburn, "A Method of Correlating Forced Convection Heat Transfer Data and a Comparison with Fluid Friction," Trans. AIChE, Vol. 29, 1933, pp. 174-210.

4. W. H. McAdams, Heat Transmission, McGraw-Hill, 1954.

5. F. W. Dittus and L. M. K. Boelter, Publications in Engineering, University of California, Berkeley Campus, Vol. 2, 1930, p. 443.

6. S. Goldstein, Modern Developments in Fluid Dynamics, First Edition, Vol. 2, Oxford Univ. Press, London, 1938, p. 631.

7. M. Sibulkin, "Heat Transfer near the Forward Stagnation Point of a Blunt Body," J. Aeronautical Sciences, August 1952.

8. F. Kreith, Principles of Heat Transfer, Second Edition, Section 5, International Textbook Co., Scranton, PA, 1965.

9. R. M. Rivello, "Thermal Stress Analysis of Sandwich Cylinders," APL/JHU TG 721, August 1965.

10. S. Timoshenko and J. N. Goodier, Theory of Elasticity, McGraw-Hill, New York, 1951.

11. R. M. Rivello, "Comparisons of Radome Stress Solutions," APL/JHU EM-3989, August 1965.

12. L. B. Weckesser et al., "Environmental Limitations of Alumina, Fused Silica, and Pyroceram 9606 Radomes," APL/JHU TG 865, May 1967.

13. R. H. Hallendorff, "Wideband Radome Antenna Research," Section 3/9, "Research and Development Quarterly Report," APL/JHU U-RQR/64-3, July-September 1964.

14. E. T. Marley and H. Ginsberg, "Supersonic Pressure Distribution and Axial Force Characteristics of Axisymmetric Noses at Angle of Attack," Paper Presented at the Seventh U.S. Navy Symposium on Aeroballistics, 7-9 June 1965.

15. G. M. Dusinberre, Heat-Transfer Calculations by Finite Differences, International Textbook Co., Scranton, PA, 1961.

16. "System 360 Model 91 User's Guide," APL/JHU BCS-1:40, November 1973.

17. "IBM OS Linkage Editor and Loader," Eleventh Edition, IBM File No. S360/S370-31, Order No. GC28-6538-10, April 1973.

LIST OF SYMBOLS

Symbol Definition and Assumed Units

A	area (ft^2)
a	sonic velocity (ft/s)
b_i	radial position
$\overline{C}$	vector of heat capacity values for each node (Btu/ft^3-°R)
C_{Nr}, C_{Ar}	normal and axial force coefficients for the radome
C_1, C_2	constants in Planck's equation (Eq.(23)) and others
c_f	friction coefficient
c_v	specific heat (Btu/lbm-°R), equal to du/dt
c_p	specific heat (Btu/lbm-°R)
d	wall thickness or length measure (in.)
D	antenna diameter (in.); arbitrary constant
E_b	black body irradiance (Btu/ft^2-s)
E_g	grey body irradiance (Btu/ft^3-s)
E_i	Young's Modulus of the ith subregion (lb/in^2)
$\Delta e/e_0$	boresight error slope (deg/deg)
F_{Nr}, F_{Ar}	normal and axial forces acting on the radome shape (lbf)
$\Delta f/f_0$	percent change in frequency
F_x, F_y	resultant forces acting on radome in x and y directions (lbf)
h_i	heat transfer coefficient (lbm/ft^2-s)
$\overline{H}$	the vector of total conductance for each node n (Btu/h-°R)
I	value of the general integral $\int F(x)dx$
i	enthalpy (Btu/lbm)
k	thermal conductivity (Btu/ft-°R-h)
K_{cc}	the net thermal conductivity between two dissimilar materials, including contact resistance (Btu/ft-°R-h)
K	number of nodes connected to node n via internal conduction

L	length measure (ft)
M	Mach number
m_r	radome mass (lbm)
M_0	resultant bending moment acting at radome's base (in.-lbf)
Nu	Nusselt number, equal to $c_p h_i x/k$
Pr	Prandtl number equal to $\mu c_p/k$
P, p	pressure (lbf/ft^2)
$\overline{Q}$	heat flow vector (Btu/h)
$\dot{q}$	magnitude of heat flow vector ($\lvert\overline{Q}\rvert$) (Btu/h)
$\dot{q}''$	generalized heat flux term (Btu/ft^2-h)
q'''	generalized heat generation term ($Btu/h-ft^3$)
Q''	the number of independent heat flux sources exchanging heat with node n
R	number of nodes connected to node n via radiation, or relaxation factor
R	gas constant (ft-lbf/lbm-°R)
R	resultant force (lbf)
R_b	radome base radius (in.)
r	radial coordinate (ft)
r	recovery factor
r	reflectivity
St	Stanton number = $\dot{q}/\rho V(i_r - i_w)$
T, $\overline{T}$	temperature (°R)
t	time (s or h)
t	thickness (in.)
u	internal energy (Btu/lbm)
V	velocity (ft/s)
V	volume (ft^3)
v	specific volume (lbm/ft^3)
x, y, z	spatial coordinates (ft)
X, Y	coordinate axes or generalized functional values (i.e., X = f(Y))
Z	compressibility of a gas

Greek Symbols

α	absorptivity
α	thermal expansion coefficient ($^\circ R^{-1}$)
$\alpha, \alpha', \beta, \beta'$	constants in heat transfer correlations
γ	ratio of specific heats
$\overline{\nabla}$	gradient vector operator (ft^{-1})
δ	error correction term ($^\circ R$)
ϵ	emissivity
ϵ	dielectric constant
θ, ϕ	angular coordinates (rad)
θ	quadrant elevation angle (rad)
λ	wavelength (in.)
μ	fluid viscosity (lbm/ft-s)
ν	Poisson's ratio
σ	Stephan-Boltzmann constant (0.174×10^{-8} Btu/ft^2-h-$^\circ R^4$)
τ	fluid/wall shear stress (lbf/in^2)
σ_z	axial direction stress (lb/in^2)
σ_θ	circumferential direction stress (lb/in^2)
σ_r	radial direction stress (lb/in^2)
ψ	electrical thickness of radome wall

INITIAL DISTRIBUTION EXTERNAL TO THE APPLIED PHYSICS LABORATORY*

The work reported in TG 1293 was done under Navy Contract N00017-72-C-4401. This work is related to Task A33, which is supported by NAVSEASYSCOM.

ORGANIZATION	LOCATION	ATTENTION	No. of Copies
DEPARTMENT OF DEFENSE			
DDC	Alexandria, VA		12
Department of the Navy			
NAVSEA	Washington, DC	SEA 03513	1
NAVAIR	Washington, DC	AIR-320B	1
Naval Air Development Ctr.	Johnsville, PA	G. J. Tatnall	1
Naval Weapons Ctr.	China Lake, CA	F. Markarian	1
Department of the Army			
Army Missile Command	Redstone Arsenal, AL	K. N. Letson	1
Department of the Air Force			
Air Force Materials Lab./LPO	Wright-Patterson AFB, OH	W. Frederick	1
CONTRACTORS			
General Dynamics, Electronics	San Diego, CA	G. Tricoles	1
General Dynamics, Pomona	Pomona, CA	D. Roberts	1
Georgia Inst. of Technology, High Temperature Materials Div.	Atlanta, GA	J. D. Walton	1
Raytheon Co., Missile Systems Div.	Bedford, MA	F. R. Youngren	1
McDonnell Douglas East	St. Louis, MO	Dr. D. C. Ruhmann	1
Hughes Aircraft	Los Angeles, CA	R. Nielsen	1

Requests for copies of this report from DoD activities and contractors should be directed to DDC, Cameron Station, Alexandria, Virginia 22314 using DDC Form 1 and, if necessary, DDC Form 55.

*Initial distribution of this document within the Applied Physics Laboratory has been made in accordance with a list on file in the APL Technical Publications Group.

SUPPLEMENTARY

INFORMATION

THE JOHNS HOPKINS UNIVERSITY
APPLIED PHYSICS LABORATORY
LAUREL MARYLAND

ERRATA SHEET FOR APL/JHU TG 1293A,

URLIM — A Unified Radome Limitations Computer Program,

Volume 1 — Theoretical Background

1. Change Eq. 35 (p. 30) to:

$$u_i|_{b_{i+1}} = u_{i+1}|_{b_{i+1}} \quad , \quad i = 1 \text{ to } (n-1) \quad , \qquad (35)$$

2. Change the third line of the paragraph following Eq. 40 (p. 31) to:

stitution of these into Eqs. (29) through (31) yields σ_{r_i}, σ_{θ_i}, and

3. Change the first line of the paragraph following Eq. 51c (p. 45) to:

The stresses caused by these forces are distributed around

4. Change the equation on the sixth line of p. 61 to:

$$-2C/r^3 + (2/r)(C/r^2) = 0 \ ,$$

5. Change the third line following Eq. 69 (p. 66) to:

$\overline{T}$. Combining Eqs. (68) and (69) yields:

6. Change the third line of the last paragraph on p. 66 to:

correction factors $(\overline{Q}_0/\overline{Q}'_0)$. The heating rate for each node $(\overline{Q})$

7. Change Eq. 75 (p. 68) to:

$$\frac{\partial k_{n-1}}{\partial T_n} = \frac{f'_1\,[(T_n + T_i)/2]}{2} \quad , \qquad (75)$$

8. Change the fourth line of the second paragraph following Eq. 76 (p. 68) to:

on the initial guess for the temperature field ($\bar{T}_0$); (2) the

9. Change the first line of the second paragraph on p. 70 to:

The above system shows nodes 1 through n as regular inter-

10. Change the eighth line on p. 74 to:

is the extent of the vector $\bar{X}_a$ then i is set to n-1. Exactly

11. Change the fifteenth line of the second paragraph on p. 79 to:

age (c.f. Appendix F of Vol. 2 of this report). When employing

12. Change the last line of the second paragraph on p. 79 to:

Vol. 2 of this report).

13. Change the seventh line on p. 87 to:

R. W. Newman and D. Brockelbank for their suggestions and assistance